Title

Cell-Taxi: Mesenchymal Cells Carry and Transport Clusters of Cancer Cells

Journal

Small, 18(50)

ISSN

1613-6810

Authors

Zarubova, Jana
Hasani-Sadrabadi, Mohammad Mahdi
Norris, Sam CP
et al.

Publication Date

2022-12-01

DOI

10.1002/smll.202203515

Peer reviewed

HHS Public Access

Author manuscript

Small. Author manuscript; available in PMC 2023 December 01.

Published in final edited form as:

Small. 2022 December ; 18(50): e2203515. doi:10.1002/smll.202203515.

Cell-Taxi: Mesenchymal Cells Carry and Transport Clusters of Cancer Cells

Jana Zarubova,
Department of Bioengineering, University of California, 420 Westwood Plaza, 5121 Engineering V, Los Angeles, CA 90095-1600, United States

Department of Biomaterials and Tissue Engineering, Institute of Physiology of the Czech Academy of Sciences, Prague, 14220, Czech Republic.

Mohammad Mahdi Hasani-Sadrabadi,
Department of Bioengineering, University of California, 420 Westwood Plaza, 5121 Engineering V, Los Angeles, CA 90095-1600, United States

Sam CP Norris,
Department of Bioengineering, University of California, 420 Westwood Plaza, 5121 Engineering V, Los Angeles, CA 90095-1600, United States

Fatemeh Sadat Majedi,
Department of Bioengineering, University of California, 420 Westwood Plaza, 5121 Engineering V, Los Angeles, CA 90095-1600, United States

Crystal Xiao,
Department of Bioengineering, University of California, 420 Westwood Plaza, 5121 Engineering V, Los Angeles, CA 90095-1600, United States

Andrea M Kasko,
Department of Bioengineering, University of California, 420 Westwood Plaza, 5121 Engineering V, Los Angeles, CA 90095-1600, United States

Song Li
Department of Bioengineering, University of California, 420 Westwood Plaza, 5121 Engineering V, Los Angeles, CA 90095-1600, United States

Abstract

Cell clusters that collectively migrate from primary tumors appear to be far more potent in forming distant metastases than single cancer cells. A better understanding of the collective cell migration phenomenon and the involvement of various cell types during this process is needed. Here, we

songli@ucla.edu .

Author Contributions

J.Z., A.K., and S.L., designed the research. J.Z., M.M.H.S., F.S.M. and S.N, C.X. performed the research. All authors performed the data analysis and interpreted the results. J.Z wrote the manuscript with input from all authors.

Competing Interest Statement

The authors declare no potential conflicts of interest with respect to the authorship and/or publication of this article.

Supporting Information

Supporting Information is available from the Wiley Online Library or from the author.

developed an *in vitro* platform based on inverted-pyramidal microwells to follow and quantify the collective migration of hundreds of tumor cell clusters at once. Our results indicate that mesenchymal stromal cells (MSCs) or cancer-associated fibroblasts (CAFs) in the heterotypic tumor cell clusters may facilitate the metastatic dissemination by transporting low-motile cancer cells in a Rac-dependent manner and that extracellular vesicles secreted by mesenchymal cells only play a minor role in this process. Furthermore, in vivo studies show that cancer cell spheroids containing MSCs or CAFs have faster spreading rate. These findings highlight the active role of co-traveling stromal cells in the collective migration of tumor cell clusters and may help us to develop better targeted therapies.

Graphical Abstract

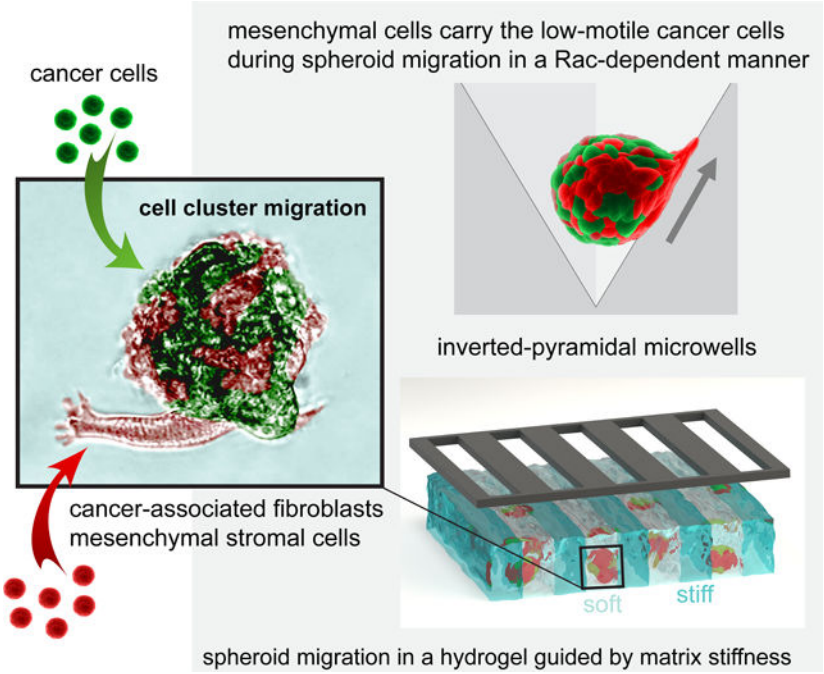

In vitro platform based on low-adhesive inverted-pyramidal microwells enables screening of cell cluster migration properties. Mesenchymal cells in small heterotypic tumor cell clusters transport low-motile cancer cells in the microwells as well as in 3D micropatterned hydrogel.

Keywords

collective cell migration; spheroid migration assay; circulating tumor cell clusters; extracellular vesicles; micropatterned hydrogel

1. Introduction

The majority of cancer-related deaths are not caused by the primary tumor, but rather by the metastatic spreading of cancer cells to distant organs.[1] Metastasis is generally described as a multistep process, in which transformed epithelial cells acquire mesenchymal features, detach from the primary tumor, migrate through a tissue to the vasculature and travel to

distant sites where they proliferate.[2] Metastases were thought to originate from single cancer cells; however, recent research suggests that up to 97% of metastases actually arise from clusters of cells that collectively migrate from the primary tumor, circulate in the blood and extravasate at distant sites. [3–6]

Migration of cancer cell groups is highly dependent on the chemical and physical guidance cues provided by the tumor stroma, which polarize cell collectives and enable their coordinated movement. For example, macrophages attracted by cancer cells can stimulate multicellular streaming of tumor cells.[7] Moreover, activated fibroblasts in tumor stroma exert forces on cancer cells[8] and create tracks[9] in extracellular matrix (ECM) or align collagen fibers[10], which promote efficient directional migration of groups of cancer cells along these features. Movement of cohesive multicellular groups is generally led by an invasive leader cell, which creates a path and sets the direction of migration for non-invasive follower cells in the group.[11]

Once the groups of cancer cells invade the vasculature, they can dynamically reorganize and adjust their geometries to pass even through narrow blood vessels.[12] These multicellular groups, also known as circulating tumor cell clusters (CTCCs), can contain between 4 – 100 cells.[12] However, CTCCs found in the bloodstream of cancer patients are not composed solely of cancer cells and may also contain mesenchymal cells, endothelial cells, and/or immune cells.[13] Clusters of mesenchymal cells with cancer cells have been detected in the peripheral blood of patients with metastatic breast cancer but not in the blood of healthy donors. The presence of circulating CAFs in the blood was confirmed in 88% of patients with metastatic disease and only in 23% of patients with localized breast cancer. [14] Similarly, increased numbers of circulating mesenchymal cells correlated with worse prognosis and a lower probability of survival in metastatic patients.[15] The importance of co-traveling mesenchymal/stromal cells in the metastatic process is also supported by observations that up to 86% of carcinoma cells that spread to the lungs were accompanied by primary tumor stroma-derived cells; in majority of cases, these cells stained positive for smooth muscle α-actin (αSMA) but only 28% cases stained positive for F4/80, a macrophage marker.[16] When the tumor stromal cells were partially depleted, the number of metastases significantly decreased.

While mesenchymal stromal cells (MSCs) are known to be recruited to damaged or inflamed tissue, where they promote tissue regeneration, MSCs are also attracted to tumor sites.[17–19] Currently, without lineage tracing experiments, it is difficult to discern CAFs from MSCs since many markers that are used to identify CAFs (α-SMA, vimentin, fibroblast activation protein (FAP)) can be also found in MSCs. [20–22] Multiple lines of evidence, however, suggest that a significant percentage (up to 30%) of CAFs in the tumor microenvironment originate from bone marrow mesenchymal cells.[23–26] The recruitment frequency of bone marrow-derived mesenchymal cells to the tumor sites seems to be dependent not only on the cancer type but also on the tumor site location.[27]

Activated mesenchymal cells of within the tumor stroma may increase cancer invasiveness by secreting matrix metalloproteinases (MMPs)[28], which are responsible for the degradation of ECM components and the release of growth factors bound to the ECM.

Studies also show that MSCs can increase cancer metastatic potential by releasing soluble factors such as chemokine CCL5[29, 30] or growth factors such as TGF-β [31] that promote the epithelial-to-mesenchymal transition (EMT) and increase cancer cell motility. However, it is not clear what role MSCs (or mesenchymal cells, in general) have in CTCCs. It is still unknown if MSCs contribute to the increased metastatic incidence through the production of paracrine factors that promote cancer EMT and by providing a favorable niche at the secondary metastatic organs or if there are other ways by which these cells participate in the metastatic dissemination of CTCCs.

To understand the role of mesenchymal cells in the collective migration of CTCCs, we develop an *in vitro* model that enables us to follow and quantify the migratory ability of hundreds of cell clusters at once. Our results suggest that the current theory of malignant cells bringing their own soil (passenger stromal cells) to the secondary metastatic sites might not be accurate. Instead, stromal cells may actively facilitate cancer cell dissemination by providing “taxi” transport of cancer cells.

2. Results

2.1. Collective migration of cell clusters is cell-type dependent

To analyze differences in the collective migration of cell clusters formed by different cell types *in vitro*, cells were seeded as single-cell suspension into low-adhesive inverted-pyramidal microwell plates at a concentration of 50 cells per microwell to form aggregates. This technique has been used to fabricate cellular aggregates of various cell types for *in vitro* cellular studies[32], fabrication of therapeutics [33], and drug screening. [34] We observed that the adhesiveness of the microwell surface affected spheroid formation and spheroid migration from the bottom to the top edge of the microwells. If no anti-adhesive coating was applied to the microwell surface, cells spread on the surface and did not form spheroids. If pre-formed spheroids were seeded on the non-coated microwells, they spread and did not move either. When the surface was incubated with an anti-adhesive solution (5% w/v Pluronic F-127) for a prolonged period of time, a completely anti-adhesive surface was created, which allowed spheroid formation but not migration. However, short incubation times (<10 minutes) with an anti-adhesive solution enabled the formation of a low-adhesive surface that not only promoted spheroid formation but also permitted cell cluster migration. To test if the spheroid migration behavior in the microwell plates was unique to the microwell topology, we examined the motility of pre-formed fibroblast spheroids on low-adhesive flat surfaces. Within micropatterned surfaces, the migrated distance and velocity of cell aggregate migration was significantly greater than on the flat surface (Figure 1a). Therefore, we used the low-adhesive micropatterned surfaces for the remainder of this study.

Depending on the cell composition of the aggregates, differences in cluster migration from the bottom to the top edge of the microwells were observed. Displacement of the spheroids was evaluated after 24 hours. Each well of a 24 well plate contained approximately 1000 microwells, which allowed for the evaluation of 1000 cell clusters simultaneously. In this study, the migration of spheroids formed by four cancer cell lines (MCF7, MDA-MB-231, 4T1, and B16-F10), macrophages, endothelial cells (ECs), fibroblasts, cancer-associated fibroblasts (CAFs) and MSCs was tested. Of these cells, spheroids containing MSCs showed

the highest migratory ability, followed by spheroids containing CAFs. A majority of the MSC spheroids reached the top of the microwell after 24 hours (Figure 1b). Interestingly, all displaced spheroids remained at the top edges of the microwells (Figure 1bi) and did not migrate back to the bottom.

Figure 1c shows analyses of spheroid motility in the low-adhesive microwells evaluated from videos of time-lapse microscopy (movie S1 and S2). The cross in the graphs represents the edges of the pyramid. As can be seen from the migration trajectories, most of the spheroids do not randomly migrate around the microwell but they choose to migrate along one of the edges or on the smooth surface of one of the four faces. Pyramidal microwells that are approximately 400 μm in length, 400 μm in width and 300 μm in depth were used for all the experiments (Figure S1). Larger-sized microwells were only used to test the migratory behavior of larger spheroids (2000 cells), which resulted in migration comparable to the smaller cell clusters (movie S3). We did not observe any significant differences in the spheroid migration among the human low metastatic breast cancer cell line (MCF7), highly metastatic breast cancer cell lines (MDA-MB-231), mouse metastatic breast cancer cell line (4T1) and melanoma (B16-F10). Likewise, EC clusters moved significantly less than mesenchymal (fibroblast, CAF, and MSC) clusters, which migrated efficiently as shown on the spheroid migration trajectories. Fibroblast, CAF, and MSC spheroids were able to migrate comparable distances (Figure 1d) but MSC clusters moved the fastest (Figure 1e). Single cancer cells (MCF7 and MDA-MB-231) seeded in the microwells moved with the same velocity as their cell aggregates, while the velocity of single MSCs was lower than the velocity of MSC aggregates (Figure S2a). If pre-formed MSC spheroids were re-seeded in new microwells (movie S4), they moved with a velocity comparable to the spheroids without re-seeding (Figure S2b).

As a reference benchmark, we also determined the effect of anti-adhesive surface coating on the single cell migration velocity of three cancer cell lines (4T1, MCF7 and MDA-MB-231) and MSCs (Figure S3). Cells were seeded either on standard tissue culture-treated plastic or on the same two-dimensional (2D) surface treated with anti-adhesive solution (5% w/v Pluronic F-127) for 10 minutes. Anti-adhesive coating increased the migration velocity of 4T1, MDA-MB-231 cancer cells and MSCs. Epithelial cancer cells (4T1 and MCF7) moved more slowly comparing to MDA-MB-231 cells. MSCs were the fastest from all the cell types tested.

2.2. Mesenchymal cells in cell clusters enable the collective migration of tumor cells

Since CTCCs are not generally composed of only cancer cells, we tested the migration of spheroids composed of a mixture of MCF7 cancer cells with another cell type in a 1:1 ratio (Figure 2a). Here, we evaluated the efficacy of spheroid migration based on the number of spheroids that migrated to the top of the microwell from their initial position after 24 hours of culture. Spheroids that moved short distances but did not reach the top of the microwell were not counted as “migrated” by this metric. Cell clusters of MCF7 with MSCs migrated the most efficiently followed by mixed spheroids of MCF7 and CAFs (movie S5). Mixed cell clusters containing monocytes, macrophages or ECs stayed at the bottom of the microwell in majority of cases (Figure 2c). The accumulated distance evaluated

from time-lapse microscopy videos for different mixed spheroids followed a similar trend and was the highest for MCF7+MSC spheroids and MCF7+CAF spheroids. Furthermore, MCF7+MSC spheroids migrated faster than MCF7+CAF spheroids, and there was no significant difference between the velocity of MCF7+CAF and MCF7+Fib spheroids.

The size of cell aggregates is another factor that might influence the collective migration. With increasing size of spheroids composed of a 1:1 ratio of cancer cells and MSCs, more migrating spheroids were detected (Figure 2d), which was apparent when comparing bigger spheroids of 100 cells with cell clusters as small as 6 cells. In all cases, MSCs and not cancer cells were in a contact with the surface of the well during cell cluster migration, which can be seen in Figure 2e. To further confirm the differences in the migration of cell clusters of different sizes, we measured the velocities of spheroids composed of just the migratory MSCs. Smaller spheroids of 12 cells (60 μm in diameter) migrated slower than the spheroids of 25 cells (80 μm in diameter) and 50 cells (90 μm in diameter), while the velocity of larger spheroids of 100 cells (110 μm in diameter) was reduced (Figure 2f).

In order to show that MSCs were transporting the low migratory cancer cells, we impaired the motility of MCF7 cancer cells and MSCs by using chemical inhibitors of Rac or Rho kinase p160ROCK. When Rac was inhibited in both cell types using the chemical inhibitor, the spheroid migration was abolished, but the inhibition of p160ROCK with Y-27632 failed to do so, suggesting that Rac-mediated cell protrusions were required for spheroid migration. To dissect the respective role of Rac in MCF7 cancer cells and MSCs, we knocked down Rac1 in MCF7 cancer cells (C-Rac) and MSCs (M-Rac) respectively (Figure 2g). Spheroids containing normal cancer cells and MSCs with silenced Rac1 (C+M-Rac) could not migrate, while spheroids containing cancer cells with Rac1 knockdown and normal MSCs (C-Rac+M) could still migrate (Figure 2h), suggesting that Rac1 in MSCs as carrier cells was essential for spheroid migration.

Rac can also regulate integrin signaling and conversely, integrin engagement can regulate the distribution and activation of Rac in the migrating cell cluster.[35] Inhibition of the intracellular kinases such as focal adhesion kinase (FAK) and Src, which are involved in the integrin signaling might be a way to internally modulate adhesion and migration properties of cells, but it may also affect the integrity of cell cluster by suppressing cadherin signaling.[36]

To find out which proteins are used as adhesion substrates by the migrating cell clusters, we have done mass spectrometry analysis of proteins deposited on the microwell surface from the medium supplemented with 10% fetal bovine serum (FBS), and we have identified fibronectin as one of the main ECM proteins (Figure S4). Therefore, we have analyzed the expression of integrin α5β1, one of the main fibronectin receptors, on the surface of cancer cells and MSCs in the spheroids. MSCs showed higher expression of integrin α5 than cancer cells while β1 integrin was elevated on both MDA-MB-231 cancer cells and MSCs (Figure S5).

2.3. Migration of tumor cell clusters is enhanced by larger proportions of MSCs in a cluster

To determine if spheroid composition, more specifically, the ratio of cancer cells to MSCs affects cell cluster migratory ability, we prepared mixed cell aggregates that contained 50 cells per spheroid with different ratios of cancer cells to MSCs. Four different cancer cell lines were examined. With increasing counts of MSCs in the spheroids, there was a significant increase in the number of cell clusters capable of migrating to the top of the microwells for all four cancer cell lines (Figure 3a–d). Spheroids containing fewer MSCs (10:1 or 5:1 for cancer cells:MSCs) were generally the least migratory. Differences among spheroids formed by different cancer cell lines were observed. Cell aggregates with lower numbers of MSCs migrated more when they were mixed with the more aggressive breast cancer cell line MDA-MB-231 compared to spheroids containing more epithelial cancer cells (MCF7 or 4T1).

Differences in the cohesion and the cell distribution inside the spheroid (Figure 3e) were observed as well. MCF7 cancer cells tended to be more segregated from MSCs. Similarly, 4T1 epithelial cancer cells were generally found in the outer layer of the spheroids, while B16-F10 cells formed well interconnected structures with MSCs. In contrast to MCF7 and 4T1 cancer cells, monocultures of MDA-MB-231 and B16-F10 cells were not able to form compact spheroids and often migrated in smaller clusters when lower concentrations of MSCs were added (movie S6). Nevertheless, even in smaller clusters, MSCs were in the contact with the surface, transporting the cancer cells. With increasing numbers of MSCs in the cell aggregates, the spheroids became more compact and migrated as a single entity.

The differences in spheroid cohesion can be also observed in Figure 3f,g (and also Figure S6) for spheroids harvested from microwells after 24 hours. All microwells contained the same number of cells (50 cells per microwell) but different ratios of cancer cells:MSCs. If cell-to-cell adhesion was the same for all cancer cells, the spheroid sizes should be comparable among all groups. This is true for spheroids containing different ratios of MCF7 (Figure 3f) and 4T1 (Figure S6a) cancer cells but not for MDA-MB-231 (Figure 3g) and B16-F10 cells (Figure S6b). The clusters of the later of these two cancer cell types fell apart when there were lower numbers of MSCs in the spheroids, and the spheroid diameter was therefore much smaller.

As the percentage of MSCs increased, we observed that the size of the spheroids decreased slightly (Figure 3f). We hypothesize that this slight decrease in spheroid size could be attributed to increased cellular forces from the MSCs that act to compress and compact the spheroid. To further test this hypothesis, we looked at the compression of cells within the spheroids as a function of distance from the spheroid centroid. We found that nuclei-to-nuclei distance was positively correlated with normalized distance from the centroid of the spheroid, $r(663) = 0.297$, $p < 0.0001$ (Figure S7). That is, nuclei-to-nuclei spacing was larger on the outside of the spheroids and smaller in the interior of the spheroids, suggesting that MSCs compressed the cells in the interior of the spheroid.

The changes in spheroid compactness dependent on the ratio of MSCs in the cell cluster can be further supported by differences in the spheroid mechanical properties (Figure S8).

Atomic force microscopy (AFM) revealed that with increasing numbers of MSCs in cell clusters, the spheroids stiffened, which could be related to the differences in the stiffness between cancer cells and MSCs and to the increased compression of the cells due to the forces exerted by MSCs because cells with larger cortical stiffness tend to exert higher contractile forces.[37]

In contrast to conventionally cultured cancer cells in 2D, cancer cells in spheroids also showed increased ability to phagocytose MSCs. Internalization of the components derived from MSCs was observed in all cancer cells tested, but prevailed in the more aggressive cell lines, mainly in melanoma cancer cells (Figure 3e).

2.4. MSC extracellular vesicles (EVs) play a minor role in MSC-mediated migration of tumor cell clusters

In addition to the migratory capability of MSCs, paracrine signals could also play a role in MSC-mediated tumor cell migration. Extracellular vesicles (EVs) are considered to mediate a majority of the paracrine effects of MSCs.[38] Therefore, we determined whether EVs secreted by MSCs affected the collective migration of tumor cell clusters. Larger microvesicles were separated from smaller EVs by differential ultracentrifugation, and EVs with a mean size of 70 nm were obtained during the final step of the isolation process after 3-hour ultracentrifugation for 100,000 × g. EVs isolated from ECs, i.e., cells that did not support cell aggregate migration in our setup, were used as a control group.

The concentration of EVs secreted by MSCs was on average 10 times higher than the concentration of EVs secreted by ECs (Figure 4a). The vesicular nature of isolated particles was confirmed by transmission electron microscopy (Figure 4b). Isolated EVs were negative for calnexin, a protein localized in endoplasmic reticulum, and positive for EV markers[39] CD63, Flot1, CD81 and CD9 (Figure 4c). The concentration of these EV markers varied depending on the cell type.

Cancer aggregates were treated with 3 different concentrations of EVs (10, 20 and 50 μg/ml) and spheroid migration was evaluated after 24 hours. Spheroids of two cancer cell lines, MCF7 and B16-F10, were tested. In both cases, we observed the same trend. With increasing concentration of MSC EVs, there was an increase in cancer spheroid migration but this effect was much weaker compared to the physical presence of MSCs in the co-culture (on average 133 migrated MCF7 spheroids from 1000 at the highest MSC EV concentration tested over 611 migrated spheroids out of 1000 when MSCs were physically present in the clusters) (Figure 4d,f). The effect of conditioned medium from MSCs did not statistically differ from the effect of the highest EV concentration tested (Figure S9). Cell clusters containing B16-F10 cancer cells showed higher responsiveness than MCF7 cell clusters to MSC EVs and migrated more even at lower concentrations of MSC EVs. EC EVs were less powerful in promoting cell cluster migration than MSC EVs but an increase in spheroid migration could still be observed, mainly at higher concentrations of EC EVs. Nevertheless, we emphasize that a million of MSCs produce around 50 μg of EVs in 24 hours but a million of ECs secrete only 10 μg. Therefore, to achieve the same effect as with MSCs, there would need to be significantly higher numbers of ECs present in the tumor. Both MSC and EC EVs also affected cancer spheroid growth in a dose dependent manner

in both cancer spheroids tested (Figure 4e,g). EC EVs increased MCF7 spheroid growth comparably to MSC EVs but in case of B16-F10 spheroids, their effect was less significant in comparison to MSC EVs.

2.5. MSCs facilitate the migration of tumor cell clusters in a 3D microenvironment

To confirm the results obtained from the studies of cell cluster migration in the low-adhesive microwells, we created a micropatterned hydrogel that enabled us to study the spheroid directional collective migration in a 3D microenvironment. For this purpose, cell aggregates were embedded in 5 wt% gelatin methacrylamide (GelMA) hydrogels with aligned stripes of softer and stiffer regions. The hydrogels were polymerized using a visible light photoinitiator [40], and the stiffness patterns were created by exposing certain regions of the gel to light for different amounts of time by using a striped photomask containing 50-μm wide opaque stripes separated by 50-μm wide transparent stripes. Regions receiving longer exposure were stiffer and regions receiving shorter exposure were softer (Figure 5a). In this way, softer, less crosslinked stripes with Young's modulus ~2kPa and stiffer stripes of 9 kPa were created (Figure 5c). In this system, the migration of cell aggregates composed of MCF7 cancer cells was compared with the behavior of cancer cell clusters treated with MSC EVs at the concentration of 50 μg/ml and with mixed spheroids of MCF7 cells with MSCs in the ratio 1:1. Collective migration of cell clusters in 3D micropatterned hydrogel was evaluated from time-lapse microscopy videos. Cancer cell aggregates or cancer spheroids treated with MSC EVs did not migrate in this system (Figure 5di) (movies S7 and S8), however, mixed spheroids containing MSCs migrated in the direction of stripes (Figure S10, movie S9), with an average speed of 0.13 μm/minute (Figure 5e). MSCs served as leader cells for migration but still maintained the adhesions with other cells in the spheroid. Suggesting that the cell taxi migration is dependent on physical coupling of cells instead of soluble signals. Interestingly, all cell aggregates in this 3D microenvironment migrated only in the softer, less crosslinked regions. The average migrated distance of mixed spheroids of MCF7+MSCs was around 100 μm within 24 hours (Figure 5f). Over time, spheroids became elongated, cell clusters reorganized, and cancer cells got to the interior of the spheroid covered by MSCs (Figure 5dii, iii).

The difference in spheroid area was evaluated after 7 days of culture. The growth of cancer cell aggregates in the microenvironment containing MSC EVs was slightly increased compared to the cancer spheroids alone. The largest spheroid area was observed in the mixed cell aggregates when MSCs were physically present in the spheroids (Figure 5g).

Together, these results indicate that MSCs might participate in the dissemination of less migratory cancer cells by transporting cell clusters, and that paracrine factors secreted by MSCs are less potent in inducing the cancer cell cluster migration but might support the cancer cell survival and proliferation.

2.6. Comparison of the effect of CAFs and MSCs on metastatic spreading of cancer cells *in vivo*

To further confirm our observations from *in vitro* experiments, an orthotopic mouse model of spontaneous breast cancer metastasis was used to test the effect of MSCs and CAFs (the

two combinations that showed the highest migratory abilities) on the metastatic spreading of cancer cells (Figure 6). Mixed spheroids of green fluorescent 4T1 cancer cells and red fluorescent MSCs were injected into mouse mammary fat pad area and co-localization of red and green fluorescence signal was evaluated after 3 days (Figure S11). At this time point, some of the injected spheroids fused together and MSC signal was localized mainly on the outer edges of the tumor. In addition, some smaller cell aggregates containing both red and green signal were visible.

Spheroids composed of luciferase-expressing 4T1 cancer cells, 4T1+CAFs and 4T1+MSCs were used to monitor the tumor progression in living animals. After a few days post-injection, cancer cell aggregates containing MSCs/CAFs started to spread into the subcutaneous space. Cancer cells that were in contact with CAFs and MSCs grew and migrated significantly more (Figure S12, S13) than cancer cells alone and formed new niches with a high number of cancer cells based on the bioluminescence intensity. The 4T1+ MSCs group showed the largest tumor spreading area on day 18 compared to 4T1 and 4T1+CAFs.

3. Discussion

Recent reports on the increased metastatic potential of CTCCs compared to single cancer cells has highlighted the importance of studying the process of collective cell migration. However, this process, mainly in the context of cancer, is generally very slow (10 to 15 μm per day [41]) and the conditions that promote CTCC migration are not well understood. *In vivo* tracking of migrating cell clusters is very challenging. Therefore, *in vitro* systems that enable the study of collective cell migration are of a great interest.

Factors such as substrate stiffness, substrate geometry, and cell adhesion ligand concentration are known to influence migration of single cells in vitro.[42] Cells tend to migrate along topographical features such as microgrooves or fibrillar structures.[43] The microwell design is providing the guidance cues for the spheroids in a form of the four edges and four faces of the inverted pyramid that helps the cell clusters to navigate and migrate in the upward direction. As can be seen from the migration trajectories (Figure 1c), most of the spheroids do not randomly migrate around the microwell but they choose to migrate along one of the edges or on the smooth surface of one of the four faces of the inverted pyramid. Once the cell cluster reaches the top edge of the microwell, it never migrates back to the bottom, probably because the rim provides better guidance cues, and the spheroid can better attach to it. Moreover, in contrast to single cells, cell clusters also tend to show enhanced directional migration.[44] In addition to substrate geometry, cell-substrate adhesion regulates dynamic cell motility. While moderate adhesion promotes dynamic cell motility, low levels of adhesion do not support cell migration, and high adhesion suppresses cell locomotion by hindering cell detachment from the substrate.[45, 46]

Thus far, there are only a few articles focused on cell aggregate migration *in vitro*, where cell cluster migration was observed either on soft 2D surfaces [47] or in soft 3D gels.[48] However, spheroid migration in both of these systems was slow and the clusters needed to be followed by time-lapse microscopy, which does not allow for high-throughput screening

of many cell aggregates at once. On the contrary, our system permits to evaluate migration simply by the end-point assessment of the spheroid migratory ability since the cell clusters reached the top of the microwell and stayed at this stationary state.

Migration of aggregates composed of various cell types tested with the use of this system showed striking differences in their motility. Leukocyte migration is generally considered adhesion-independent. However, neither monocytes, nor macrophages migrated on these low-adhesive microwell surfaces. This might be due to the lack of confinement that is thought to be necessary for the efficient amoeboid migration.[49] We did not observe any significant motility of cancer, epithelial or endothelial spheroids within 24 hours. Clusters containing mesenchymal cells migrated efficiently as a majority of the clusters reached the top edge of the microwell in less than 24 hours.

When mixed spheroids of cancer cells and mesenchymal cells were formed, mesenchymal cells were able to transport the low-motile cancer cells to the top of the microwell. We further confirm that the cell cluster migration is dependent on mesenchymal cells by knocking down Rac1 in either cancer cells or MSCs. Silencing Rac1 in MSCs leads to the complete abolishment of spheroid migration while impairing cancer cell motility only slightly lowers the numbers of migrating spheroids. Nevertheless, the situation in vivo might not always favor mesenchymal type of collective migration. There are also reports on tumor clusters with inverted apico-basolateral polarity[48], which display a persistent amoeboid migration in confined non-adhesive environments[50] and for which evaluation our *in vitro* microwell system might not be suitable.

Cells have been reported to be able to transport cargos such as cellular backpacks, which are engineered particles conjugated to the cell surface.[51] The novelty of our work lies in the observation that mesenchymal cells can provide “cell-taxi transport” to low-motile cancer cells. Similar phenomenon can be found in the *Drosophila melanogaster* ovary, where a handful of migratory border cells transport a pair of non-motile polar cells.[52] In agreement with the collective migration in Drosophila ovary[53], in our system we have also observed the dependence of migration speed on the size of cell clusters. The number of spheroids that managed to reach the top of the microwell in 24 hours was the highest for the biggest spheroids of 100 cells. Moreover, spheroid size was positively correlated with migration speed, up to a cluster size of approximately 90 μm. Based on the previously published theoretical model[53], these data suggest that the collective migration in our microwell system may be more similar to the 3D than to the 2D environment. The biphasic dependence of velocity on the cell cluster size likely reflects a balance among several factors that contribute to the resulting migratory behavior. As collective migration is an energetically demanding process, one of the factors is the number of cells in a cluster that can serve as a driving force for cell cluster migration. Other factors include cell polarization/probing, coordination for persistent migration, cell aggregate spreading and interactions with the microenvironment. For example, if the cell aggregates are too big, the increase of aggregate spreading and probing in multiple directions may compromise the velocity of aggregate migration, as observed in Figure 2f.

The number of cells in cell aggregate is, however, not the only factor that can influence the size of cell spheroid. The compactness of cell aggregate is dependent on multiple mechanisms such as cell–ECM and cell–cell interactions as well as cellular contractility.[54, 55] For example, mesenchymal cells generally have higher contractility, and the presence of MSCs in the mixed tumor cluster makes the spheroid more compact so that even the otherwise loosely adhesive cancer cells such as B16-F10 or MDA-MB-231 migrate in clusters and not as single cells. It is worth noting that this mechanism of spheroid compaction is also dependent on the interactions between mesenchymal cells and cancer cells. Cohesive cell cluster may more efficiently transport the non-motile cells and is likely to better withstand the shear forces in the bloodstream and successfully reach the target destination.

In contrast to 2D cultures, cancer cells in 3D spheroids without contact to the surrounding ECM readily internalize components derived from MSCs or even engulf entire cells, which can give them further survival advantage in the form of nutrients derived from MSCs[56] or change their migratory properties. We, therefore, looked if paracrine factors, mainly small EVs, secreted by MSCs could promote migration of cancer spheroids. MSC EVs enhanced cancer spheroid metabolic activity by approximately 60% and increased the number of migrating cancer aggregates by 13–20% at the highest concentrations tested, which is significantly less than when MSCs were physically present in the cell cluster.

We were further interested if the behavior observed on the micropatterned surfaces reflects cell behavior in 3D microenvironment. Our *in vitro* system does not attempt to model the entire complexity of the tumor microenvironment but it is based on the observation that the collective cell migration is induced in confined spaces.[57] By utilizing photolithographic techniques, we spatially controlled the crosslink density of GelMA hydrogels and created alternating stripes with more and less crosslinking. We observed that cell clusters moved only in the softer regions. This observation is in agreement with previously published studies showing that cells choose the path of least resistance[58–60] and lowest energetic cost while navigating through a heterogenous microenvironment. [61]

In this system, we did not observe any collective migration of cancer cell clusters or cancer cell clusters treated with MSC EVs. Similarly, others have demonstrated that fibroblast-conditioned media was not able to promote cancer cell invasion and that fibroblasts needed to be physically present in the co-culture in order to lead the collective invasion or create tracks for cancer cells.[9] However, the effect of stromal EVs might be further multiplied *in vivo.* For example, EV internalization by immune cells might induce additional reactions that cannot be addressed by the two-component *in vitro* system.

Cell cluster migration was observed only in samples containing both MCF7 cancer cells and MSCs. In all cases, MSCs were the leading cells and from the time-lapse videos, it seems that even one cell can carry the entire cluster (movie S9). It is, however, possible that similarly to the tip cells in sprouting capillaries[62], one mesenchymal cell does not lead the migration the entire time but is dynamically exchanged with other mesenchymal cells.

In a mouse model of orthotopic metastatic breast cancer, we also observed that the presence of mesenchymal cells (CAFs or MSCs) in the spheroids significantly increased cancer growth and metastatic spreading compared to cancer spheroids alone, even though the administrated mixed spheroids contained just half the number of cancer cells. Tumor spreading area was higher when MSCs were included versus CAFs, which is in agreement with our *in vitro* results that highlighted the superior migratory abilities of MSCs. These findings are also consistent with a previous observation that administration of highly migratory cancer cells did not promote more aggressive tumor growth or increased metastases.[63] In addition, research in zebrafish showed that CAFs were able to hijack cancer cells where a majority of tumor cells remained in tight association with CAFs in circulation.[64] Cell-taxi effect provided by mesenchymal cells may thus be one of many factors that contribute to increased cancer cell spreading in vivo, and zebrafish might be a suitable model to study the mechanism of this specific type of collective cell migration in vivo in more details because it enables to visualize the cell cluster migration in much higher resolution.

4. Conclusion

Our study has contributed to the evidence that cancer spreading is not a process dependent on the migratory abilities of cancer cells alone. Here, we showed that even the low-motile cancer cells can be transported by more migratory mesenchymal cells, which highlights the need to better understand the behavior of other cell types that might be involved in the tumor dissemination. Furthermore, it also implies the risks of using MSCs in regenerative therapies after tumor removal as it might lead to the increased metastatic spreading of cancer cells.

5. Experimental Section/Methods

Chemicals and biologicals:

Unless noted otherwise, all chemicals were purchased from Sigma-Aldrich, Inc. Cell culture reagents, solutions, and dishes were obtained from Thermo Fisher Scientific, except as indicated otherwise. Gelatin methacrylamide was fabricated using gelatin from fish (J. T. Baker, 250 bloom) as previously described.[65]

Cells:

Cancer cell lines MCF-7, MDA-MB-231 and 4T1-Luc are from the American Type Culture Collection (ATCC, Manassas, VA). GFP expressing B16-F10 cells were obtained from Creative Biogene (Shirley, NY, USA). Unless otherwise stated, all cells were cultured in Dulbecco's Modified Eagle's Medium (DMEM) with 10% fetal bovine serum (FBS) (Gibco) and 1% penicillin/streptomycin (Gibco). RAW 264.7 macrophages as well as THP-1 monocytes were obtained from ATCC (Manassas, VA). THP-1 were cultured in RPMI-1640 medium with 10% FBS. Primary human dermal fibroblasts as well as human umbilical vein endothelial cells (ECs) were purchased from ATCC. Endothelial cells were cultured in EGM-2 medium (Lonza). Human breast cancer-associated fibroblasts (CAFs) were ordered from Cell Biologics. Human mesenchymal stromal cells (MSCs) were obtained from Texas A&M Health Science Centre College of Medicine. CAFs, MSCs, and ECs in a passage 2–5

were used in this study. In short-term co-cultures, MSCs were stained with red and cancer cells with green CellTracker (Invitrogen) according to the manufacturer's instructions. For long-term co-cultures, MSCs were transduced to stably express LifeAct-RFP using the lentiviral vector (pTwist Lenti CMV Puro) backbone (Twist Bioscience). MCF7 cancer cells were transduced to stably express LifeAct-GFP using the same lentiviral vector backbone. To generate stable Rac1 knockdowns, cells were infected with Rac1 short hairpin RNA lentiviral particles (Santa Cruz Biotechnology, Dallas, TX, USA) and then selected in medium containing 5 μg/ml puromycin. Rac1 depletion was confirmed by Western blot analysis. Rac inhibitor, ML141 was purchased from MilliporeSigma, ROCK inhibitor Y-27632 was purchased from Cayman Chemical.

Analysis of the Anti-adherence rinsing solution:

A defined volume of Anti-adherence rinsing solution (STEMCELL Technologies) was evaporated and weighed to measure the concentration. The pellets for transmission IR spectroscopy were prepared by compressing of 1mg of sample in 200 mg of potassium bromide. Transmission IR spectra of samples were measured by Cary 600 Series FTIR Spectrometer (Agilent Technologies, USA). Spectral resolution was 2 cm-1 and 128 scans were collected. The Anti-adherence rinsing solution was identified as 5% w/v Pluronic F-127 (Figure S14).

Mass spectrometry analysis:

Microwells were treated with Anti-Adherence Rinsing Solution, washed twice and incubated with the medium for 2 hours. Consequently, the medium was removed, wells were washed twice with PBS and the deposited proteins were collected in PBS by pipetting up and down 10x. 3 samples were analyzed. Proteins in solution (50 μL) were reduced by 5 mM TCEP at 56°C for 1 hour, and alkylated by 40 mM iodoacetamide at room temperature for 30 min in the dark. 200 μL of cold acetone was added to the protein solution and stored in −20°C for 1 hour before centrifugation at 13k g for 10min at 4°C. Supernatant was removed and protein pellets were air dried for 10 minutes in room temperature. Trypsin dissolved in 50 mM ammonium bicarbonate was added to protein pellets for digestion at 37°C overnight. Protein digests were desalted by Empore stage-tip the following day. Eluate from the stage-tip was dried by speed vac and re-suspended in 3% acetonitrile with 0.1% formic acid. LC MS/MS: 1.0 μg protein was injected to an ultimate 3000 nano LC, which was equipped with a 75μm × 2 cm trap column packed with C18 3-μm bulk resins (Acclaim PepMap 100, Thermo Scientific) and a 75μm × 15 cm analytical column with C18 2-μm resins (Acclaim PepMap RSLC, Thermo Scientifc). The nanoLC gradient was 3−35% solvent B (A = H2O with 0.1% formic acid; B = acetonitrile with 0.1% formic acid) over 40 minutes and from 35% to 85% solvent B in 5 minutes at flow rate 300 nL/minute. The nannoLC was coupled with a Q Exactive Plus orbitrap mass spectrometer (Thermo Fisher Scientific, San Jose, CA). The ESI voltage was set at 1.9 kV, and the capillary temperature was set at 275°C. Full spectra (m/z 350 – 2000) were acquired in profile mode with resolution 70,000 at m/z 200 with an automated gain control (AGC) target of 3×10^6. The most abundance 15 ions were subjected to fragmentation by higher-energy collisional dissociation (HCD) with normalized collisional energy of 25. MS/MS spectra were acquired in centroid mode with resolution 17,500 at m/z 200. The AGC target for fragment ions are set at 2×10^4 with maximum

injection time of 50 ms. Charge states 1, 7, 8, and unassigned were excluded from tandem MS experiments. Dynamic exclusion was set at 45.0 s.

Spheroid formation and migration:

The majority of the microwell experiments were performed using the AggreWell 400 (STEMCELL Technologies) microwell dishes. Microwells were incubated with Anti-Adherence Rinsing Solution (STEMCELL Technologies) for 5 minutes, followed by 5-minute centrifugation at 2000 × g. The wells were washed twice with medium without FBS then filled with 0.5 ml complete medium containing 10% FBS. To form spheroids containing 50 cells each, 60 000 cells were seeded per well for a 24-well plate with a final volume of 1ml of medium containing 10% FBS. Seeded cells were centrifuged for 2 minutes at 100 × g and an even cell distribution at the bottom of the microwells was confirmed under the microscope. The variation in the numbers of cells per microwell was generally 50 ± 8 cells. To evaluate the migration of spheroids formed by different cell types, time-lapse microscopy was performed at a rate of one frame every 4 or 8 minutes. Spheroid migration was manually tracked using ImageJ, the tracking was stopped once spheroid reached the top of the microwell. Cell cluster migration was evaluated using the Chemotaxis and Migration Tool (Ibidi). In other experiments, spheroid migration was evaluated by counting the number of spheroids that reached the top of the microwell after 24h. Cell metabolic activity was measured using the PrestoBlue Reagent (Invitrogen) according to the manufacturer's instructions.

For single cell migration tracking, cells were seeded in the Incucyte Imagelock 96-well Plate (some of the wells were treated for 10 minutes with Anti-Adherence Rinsing Solution). The cell migration was followed for 24h by Incucyte device. Single cell migration was manually tracked using ImageJ and evaluated using the Chemotaxis and Migration Tool (Ibidi).

Flow cytometry:

Spheroids were collected from the microwells after 24 hours, washed with PBS without Ca^{2+}, Mg^{2+}, disintegrated into single cells by 15-minute incubation in TrypLE solution (Gibco) and through pipetting. Single cells were stained with Zombie Violet Fixable Viability Kit (BioLegend), washed with PBS and stained for 30 minutes with anti-human CD29 and CD49e antibodies (BioLegend). Sample acquisition was performed on Attune NxT flow cytometer and the data were analyzed with FlowJo software (TreeStar).

Spheroid Analysis:

Spheroid size distribution was analyzed using CellProfiler and a custom pipeline to detect the spheroid boundaries. Segmented objects with a diameter of 40 μm or less were discarded since they represented single or double cells, which we do not consider as spheroids.

To measure cell compactness in the spheroid, six different MSC spheroids were imaged with a confocal microscope (Zeiss LSM880 with 40x/1.2 water immersion objective). The spheroids were imaged so that the full spheroid volume was included. The nuclei were segmented and identified using a custom pipeline in CellProfiler. For each nucleus, the distance to the first and second closest neighboring nuclei was determined and the two

distances were averaged to give the nuclei-to-nuclei spacing in microns. Since each of the six spheroids had a slightly different size, the nuclei distance to the spheroid centroid was normalized to the to the most distant nucleus in each of the six spheroids.

Atomic force microscopy (AFM) analysis of spheroids:

For mechanical characterization of the spheroids, standard V-shaped gold-coated silicon nitride tipless AFM cantilevers (BrukerNano, Camarillo, CA) were used after modification with latex beads (10 μm in diameter). The cantilever spring constant was measured using the thermal fluctuations method. The spring constant of the cantilevers used in this work was found to be 0.134 N/m. Measurements were performed using a Veeco AFM II Dimension 3100 (Veeco Metrology Inc., now BrukerNano) instrument in liquid mode. The force displacement curves were recorded with a vertical ramp size of 5 μm. To minimize viscoelastic effects, force-indentation curves were recorded at a frequency of 1 Hz.

Extracellular vesicle (EV) isolation:

EV-depleted FBS was obtained by 18h ultracentrifugation at 100,000 × g, 4 °C. Cells were washed with phosphate buffered saline (PBS) and cultured in medium containing EV-depleted FS for 24h. For all EV isolations, cell viability was higher than 95%. Conditioned medium containing EVs was centrifuged at 2,000 × g for 10 min, filtered through 0.22 μm filter, concentrated with a 10kDa Centricon Plus-70 centrifugal filter (UFC701008, Sigma Millipore) and centrifuged at 100,000 × g for 3 h at 4 °C. The EV pellet was resuspended in 100 μl PBS and stored in −80 °C until further use.

Western blotting analysis of EVs:

Cells were lysed in RIPA buffer with protease inhibitors (HALT™ Protease Inhibitor Cocktail, EDTA-free (100X), Thermo Scientific, 87785) for 20 min on ice, and were then centrifuged for 15 min at 14,000 g. The protein concentration was measured by Micro-BCA (Thermo Scientific, 23235) in the presence of 0.2 % SDS. For SDS-PAGE, samples were mixed with Laemmli Sample Buffer, boiled for 5 min at 95°C, and separated on 4–20% gradient polyacrylamide gels (4561094, Bio-Rad) before they were transferred to the PVDF membranes. The membranes were blocked with 5% non-fat milk for 1h and were then incubated overnight at 4°C with primary antibodies: anti-CANX (1:500, rabbit polyclonal anti-human ABclonal, A15631); anti-CD63 (1:500, mouse monoclonal anti-human CD63 antibody, MEM-259, abcam, ab8219); anti-FLOT1 (1:500, rabbit polyclonal anti-human ABclonal, A6220); anti-CD81 (1:300, mouse monoclonal anti-human CD81 antibody, Invitrogen, MA5–13548); anti-CD9 (1:500, mouse monoclonal anti-human CD9, clone MM2/57, Invitrogen, AHS0902). The membranes were then washed three times with 0.1% Tween 20 in PBS for 5 minutes at room temperature, and were incubated with secondary antibody conjugated to horseradish peroxidase (donkey anti-rabbit IgG-HRP, sc-2313, or donkey anti-mouse IgG-HRP, sc-2314, Santa Cruz Biotechnology) for 2 hours at 4°C. After the membranes had been washed three times with 0.1% Tween 20 in PBS, proteins were visualized with a chemiluminescence substrate (SuperSignal West Femto Maximum Sensitivity Substrate, Thermo Scientific, 34095).

Transmission electron microscopy (TEM) of EVs:

Undiluted suspensions of EVs were suspended on grids with a thin formvar/carbon film and were allowed to adsorb for 20 minutes. Excess liquid was blotted away with filter paper and the grids were then washed three times with 20 mM HEPES and 150 mM NaCl and were negatively stained with 0.4% uranyl acetate, 3% methylcelulose for 1 minute. Excess solution was blotted away, and the grids were air-dried. Samples were imaged using JEOL JEM 1200 EX operated at 120 kV.

Microfluidic Resistive Pulse Sensing analysis of EVs:

The concentration and the size distribution of EVs was analyzed by microfluidic resistive pulse sensing using Spectradyne nCS1 (Spectradyne LLC) with C-400/TS-400 cartridge.

Fabrication and characterization of hydrogels with micropatterned stiffness:

Hydrogels were covalently adhered to a glass substrate as previously described.[40] Briefly, round pieces of coverglass (12 mm in diameter, Fisher) were functionalized with methacrylate groups using the following procedure. The coverglass was first cleaned and activated with oxygen plasma (Plasma Prep II, SPI Supplies) for 5 minutes. The activated coverglass was then reacted with 3-(trimethoxysilyl)propyl methacrylate (0.5 mL) in 25 mL of an ethanol and acetic acid solution for 30 minutes. The coated coverglass was then washed with methanol three times before drying. Silanized coverglass pieces were used within two hours of functionalization.

Glass slides were rendered hydrophobic, and thus non-adherent to the polymerized hydrogels, by wiping a drop of Gel Slick (Lonza) on the slide surface. This process was repeated once to ensure a sufficient coating. The slides were then briefly rinsed with DI water to clean the surface and dried before use.

Photopolymerizable gelatin-based hydrogels were prepared using gelatin methacrylamide (GelMA) and a visible-light photoinitiator lithium phenyl-2,4,6-trimethylbenzoylphosphinate (LAP) [40]. A pre-polymer solution of 5.0 w/w% GelMA with 0.10 w/w% LAP in PBS was prepared and pipetted (10 μL/gel) between a hydrophobically modified glass slide and 12 mm round glass coverslips functionalized with methacrylate groups that were separated by 200 μm spacers. For spheroid encapsulation studies, spheroids were mixed with the pre-polymer solutions, while maintaining 5.0 w/w% GelMA and 0.10 w/w% LAP and immediately polymerized with spheroids *in situ* into a hydrogel using a collimated light source (EXFO Omnicure S1000) filtered with a 405 nm bandpass filter (Newport) with an output intensity of 4.8 mW/cm^2 as measured by a spectroradiometer (International Light Technologies, ILT950) between 350 and 500 nm. Photomasks (CAD/Art Services) with stripes of 50 μm opaque regions and 50 μm wide transparent regions were used to block light from reaching certain regions of the gels so that certain sections received 37.5 seconds exposure while others received 150 seconds exposure. These spatially defined differences in photopolymerization time led differences in crosslink density, thus, gels with spatially defined differences in elastic modulus were produced. After polymerization, the coverglass (with the attached hydrogel) was pried off the glass slide, and submersed in cell culture media. Collective migration of cells in the micropatterned gels was evaluated after 7

days when spheroids were fixed with 4% paraformaldehyde and permeabilized with 0.05% Triton X-100 and 1% bovine serum albumin solution for 15 min at room temperature. Nuclei were stained with DAPI. Images were taken on Leica SP8 confocal microscope and were evaluated using ImageJ.

The elastic modulus of both 150 second (stiff) and 37.5 second (soft) exposed regions were measured using Atomic Force Microscopy (AFM) in PBS using a JPK Nanowizard 4a BioScience AFM using the force spectroscopy mode. A CP-qp-CONT-SiO-B probe with a 3.5 μm diameter SiO_2 sphere (sQube®) was used to indent the samples. For the quantitative measurements of Young's modulus, the spring constant of the cantilever was measured using the AFM's internal contact-free thermal tuning method. Single indentations were performed with a total force of 4.0 nN. At least 15 indentations were performed at 15 different locations across the gel surface for each region. The photomasks contained fiduciary markers so that the softer and stiffer regions of the hydrogels could be correctly identified. All AFM force curve analysis was performed using the JPK Data Processing software. The Young's modulus was calculated by using a Hertz/Sneddon spherical fit with a Poisson's ratio of $\nu = 0.5$[66].

Tumor Assays:

BALB/c female mice were purchased from the Jackson Laboratory. Mouse studies were carried out under the protocols approved by the Institutional Animal Care and Use Committee at the University of California, Los Angeles. Spheroids of 50 cells composed solely of 4T1-Luc cancer cells or 4T1-Luc cells with MSCs or CAFs in the ratio 1:1 (2×10^5 cells per injection) were subcutaneously injected (100 μl per animal) into right flanks of balb/c wild-type mice (6–8 weeks old). Tumor size was assessed over time using a digital caliber as well monitored by measuring and quantifying the bioluminescence signal with the IVIS Imaging System (Perkin Elmer) until day 18 at which animals were sacrificed. Stable signals were determined by monitoring the photon count up to 30 minutes after intraperitoneal injection of luciferase substrate, D-luciferin (15 mg/ml in PBS), into animals anesthetized with 2.5% isoflurane. The Living Image software was used to acquire and analyze the bioluminescence flux data.

Statistical analysis:

One-way ANOVA with Tukey's post-hoc test or Kruskal-Wallis rank sum test were used to determine significant differences across multiple samples. Student's t-test was employed when comparisons involved only two groups.

Supplementary Material

Refer to Web version on PubMed Central for supplementary material.

Acknowledgements

This work was supported in part by grants from the National Institute of Health (R01CA234343 and R56DE029157) and Eli and Edythe Broad Center of Regenerative Medicine and Stem Cell Research Innovation Award at UCLA. We also acknowledge the Molecular Instrumentation Center, Dept of Chemistry, UCLA for mass spectrometry analysis of our samples.

References

1. Dillekås H; Rogers MS; Straume O, Cancer Med 2019, 8 (12), 5574–5576. DOI 10.1002/cam4.2474. [PubMed: 31397113]
2. Valastyan S; Weinberg RA, Cell 2011, 147 (2), 275–292. [PubMed: 22000009]
3. Cheung KJ; Ewald AJ, Science 2016, 352 (6282), 167–169. DOI 10.1126/science.aaf6546. [PubMed: 27124449]
4. Cheung KJ; Padmanaban V; Silvestri V; Schipper K; Cohen JD; Fairchild AN; Gorin MA; Verdone JE; Pienta KJ; Bader JS; Ewald AJ, Proceedings of the National Academy of Sciences 2016, 113 (7), E854–E863. DOI 10.1073/pnas.1508541113.
5. Aceto N; Bardia A; Miyamoto DT; Donaldson MC; Wittner BS; Spencer JA; Yu M; Pely A; Engstrom A; Zhu H; Brannigan BW; Kapur R; Stott SL; Shioda T; Ramaswamy S; Ting DT; Lin CP; Toner M; Haber DA; Maheswaran S, Cell 2014, 158 (5), 1110–1122. DOI 10.1016/j.cell.2014.07.013. [PubMed: 25171411]
6. Maddipati R; Stanger BZ, Cancer Discovery 2015, 5 (10), 1086–1097. DOI 10.1158/2159-8290.cd-15-0120. [PubMed: 26209539]
7. Goswami S; Sahai E; Wyckoff JB; Cammer M; Cox D; Pixley FJ; Stanley ER; Segall JE; Condeelis JS, Cancer Research 2005, 65 (12), 5278–5283. DOI 10.1158/0008-5472.can-04-1853. [PubMed: 15958574]
8. Labernadie A; Kato T; Brugues A; Serra-Picamal X; Derzsi S; Arwert E; Weston A; Gonzalez-Tarrago V; Elosegui-Artola A; Albertazzi L; Alcaraz J; Roca-Cusachs P; Sahai E; Trepat X, Nat Cell Biol 2017, 19 (3), 224–237. DOI 10.1038/ncb3478. [PubMed: 28218910]
9. Gaggioli C; Hooper S; Hidalgo-Carcedo C; Grosse R; Marshall JF; Harrington K; Sahai E, Nature Cell Biology 2007, 9 (12), 1392–1400. DOI 10.1038/ncb1658. [PubMed: 18037882]
10. Barbazán J; Matic Vignjevic D, Current Opinion in Cell Biology 2019, 56, 71–79. DOI 10.1016/j.ceb.2018.09.002. [PubMed: 30308331]
11. Summerbell ER; Mouw JK; Bell JSK; Knippler CM; Pedro B; Arnst JL; Khatib TO; Commander R; Barwick BG; Konen J; Dwivedi B; Seby S; Kowalski J; Vertino PM; Marcus AI, Science Advances 2020, 6 (30), eaaz6197. DOI 10.1126/sciadv.aaz6197. [PubMed: 32832657]
12. Au SH; Storey BD; Moore JC; Tang Q; Chen Y-L; Javaid S; Sarioglu AF; Sullivan R; Madden MW; O'Keefe R; Haber DA; Maheswaran S; Langenau DM; Stott SL; Toner M, Proceedings of the National Academy of Sciences of the United States of America 2016, 113 (18), 4947–4952. DOI 10.1073/pnas.1524448113. [PubMed: 27091969]
13. Hong Y; Fang F; Zhang Q, Int J Oncol 2016, 49 (6), 2206–2216. DOI 10.3892/ijo.2016.3747. [PubMed: 27779656]
14. Ao Z; Shah SH; Machlin LM; Parajuli R; Miller PC; Rawal S; Williams AJ; Cote RJ; Lippman ME; Datar RH; El-Ashry D, Cancer Research 2015, 75 (22), 4681–4687. DOI 10.1158/0008-5472.can-15-1633. [PubMed: 26471358]
15. Ortiz-Otero N; Marshall JR; Lash B; King MR, BMC Cancer 2020, 20 (1), 873. DOI 10.1186/s12885-020-07376-1. [PubMed: 32917154]
16. Duda DG; Duyverman AMMJ; Kohno M; Snuderl M; Steller EJA; Fukumura D; Jain RK, Proceedings of the National Academy of Sciences 2010, 107 (50), 21677–21682. DOI 10.1073/pnas.1016234107.
17. Cuiffo BG; Karnoub AE, Cell Adhesion & Migration 2012, 6 (3), 220–230. DOI 10.4161/cam.20875. [PubMed: 22863739]
18. Spaeth E; Klopp A; Dembinski J; Andreeff M; Marini F, Gene Therapy 2008, 15 (10), 730–738. DOI 10.1038/gt.2008.39. [PubMed: 18401438]
19. Chaturvedi P; Gilkes DM; Wong CCL; Kshitiz; Luo W; Zhang H; Wei H; Takano N; Schito L; Levchenko A; Semenza GL, The Journal of Clinical Investigation 2013, 123 (1), 189–205. DOI 10.1172/JCI64993. [PubMed: 23318994]
20. Chung KM; Hsu SC; Chu YR; Lin MY; Jiaang WT; Chen RH; Chen X, PLoS One 2014, 9 (2), e88772. DOI 10.1371/journal.pone.0088772. [PubMed: 24551161]

21. Talele NP; Fradette J; Davies JE; Kapus A; Hinz B, Stem cell reports 2015, 4 (6), 1016–1030. DOI 10.1016/j.stemcr.2015.05.004. [PubMed: 26028530]
22. Sharma P; Bolten ZT; Wagner DR; Hsieh AH, Ann Biomed Eng 2017, 45 (5), 1365–1374. DOI 10.1007/s10439-016-1787-z. [PubMed: 28091965]
23. Shinagawa K; Kitadai Y; Tanaka M; Sumida T; Kodama M; Higashi Y; Tanaka S; Yasui W; Chayama K, International Journal of Cancer 2010, 127 (10), 2323–2333. DOI 10.1002/ijc.25440. [PubMed: 20473928]
24. Quante M; Tu SP; Tomita H; Gonda T; Wang SSW; Takashi S; Baik GH; Shibata W; DiPrete B; Betz KS; Friedman R; Varro A; Tycko B; Wang TC, Cancer Cell 2011, 19 (2), 257–272. DOI 10.1016/j.ccr.2011.01.020. [PubMed: 21316604]
25. Ishii G; Sangai T; Oda T; Aoyagi Y; Hasebe T; Kanomata N; Endoh Y; Okumura C; Okuhara Y; Magae J; Emura M; Ochiya T; Ochiai A, Biochemical and Biophysical Research Communications 2003, 309 (1), 232–240. DOI 10.1016/S0006-291X(03)01544-4. [PubMed: 12943687]
26. Direkze NC; Hodivala-Dilke K; Jeffery R; Hunt T; Poulsom R; Oukrif D; Alison MR; Wright NA, Cancer Research 2004, 64 (23), 8492–8495. DOI 10.1158/0008-5472.can-04-1708. [PubMed: 15574751]
27. Sangai T; Ishii G; Kodama K; Miyamoto S. i.; Aoyagi Y; Ito T; Magae J; Sasaki H; Nagashima T; Miyazaki M; Ochiai A, International Journal of Cancer 2005, 115 (6), 885–892. DOI 10.1002/ijc.20969. [PubMed: 15729726]
28. Kalluri R, Nature Reviews Cancer 2016, 16 (9), 582–598. DOI 10.1038/nrc.2016.73. [PubMed: 27550820]
29. Karnoub AE; Dash AB; Vo AP; Sullivan A; Brooks MW; Bell GW; Richardson AL; Polyak K; Tubo R; Weinberg RA, Nature 2007, 449 (7162), 557–563. DOI 10.1038/nature06188. [PubMed: 17914389]
30. Zhong W; Tong Y; Li Y; Yuan J; Hu S; Hu T; Song G, Oncotarget 2017, 8 (43), 73693–73704. DOI 10.18632/oncotarget.17793. [PubMed: 29088737]
31. Ridge SM; Sullivan FJ; Glynn SA, Molecular Cancer 2017, 16 (1), 31. DOI 10.1186/s12943-017-0597-8. [PubMed: 28148268]
32. Stevens K; Ungrin M; Schwartz R; Ng S; Carvalho B; Christine K; Chaturvedi R; Li C; Zandstra P; Chen C, Nature communications 2013, 4 (1), 1–11.
33. Nguyen AH; Wang Y; White DE; Platt MO; McDevitt TC, Biomaterials 2016, 76, 66–75. [PubMed: 26519649]
34. Mosaad E; Chambers K; Futrega K; Clements J; Doran M, Scientific reports 2018, 8 (1), 1–12. [PubMed: 29311619]
35. Yamaguchi N; Mizutani T; Kawabata K; Haga H, Scientific Reports 2015, 5 (1), 7656. DOI 10.1038/srep07656. [PubMed: 25563751]
36. Canel M; Serrels A; Miller D; Timpson P; Serrels B; Frame MC; Brunton VG, Cancer Research 2010, 70 (22), 9413–9422. DOI 10.1158/0008-5472.can-10-1454. [PubMed: 21045155]
37. Das A; Monteiro M; Barai A; Kumar S; Sen S, Scientific Reports 2017, 7 (1), 14219. DOI 10.1038/s41598-017-14340-w. [PubMed: 29079818]
38. Witwer KW; Van Balkom BWM; Bruno S; Choo A; Dominici M; Gimona M; Hill AF; De Kleijn D; Koh M; Lai RC; Mitsialis SA; Ortiz LA; Rohde E; Asada T; Toh WS; Weiss DJ; Zheng L; Giebel B; Lim SK, Journal of extracellular vesicles 2019, 8 (1), 1609206–1609206. DOI 10.1080/20013078.2019.1609206. [PubMed: 31069028]
39. Thery C; Witwer KW; Aikawa E; Alcaraz MJ; Anderson JD; Andriantsitohaina R; Antoniou A; Arab T; Archer F; Atkin-Smith GK; Ayre DC; Bach JM; Bachurski D; Baharvand H; Balaj L; Baldacchino S; Bauer NN; Baxter AA; Bebawy M; Beckham C; Bedina Zavec A; Benmoussa A; Berardi AC; Bergese P; Bielska E; Blenkiron C; Bobis-Wozowicz S; Boilard E; Boireau W; Bongiovanni A; Borras FE; Bosch S; Boulanger CM; Breakefield X; Breglio AM; Brennan MA; Brigstock DR; Brisson A; Broekman ML; Bromberg JF; Bryl-Gorecka P; Buch S; Buck AH; Burger D; Busatto S; Buschmann D; Bussolati B; Buzas EI; Byrd JB; Camussi G; Carter DR; Caruso S; Chamley LW; Chang YT; Chen C; Chen S; Cheng L; Chin AR; Clayton A; Clerici SP; Cocks A; Cocucci E; Coffey RJ; Cordeiro-da-Silva A; Couch Y; Coumans FA; Coyle B; Crescitelli R; Criado MF; D'Souza-Schorey C; Das S; Datta Chaudhuri A; de Candia P; De

Santana EF; De Wever O; Del Portillo HA; Demaret T; Deville S; Devitt A; Dhondt B; Di Vizio D; Dieterich LC; Dolo V; Dominguez Rubio AP; Dominici M; Dourado MR; Driedonks TA; Duarte FV; Duncan HM; Eichenberger RM; Ekstrom K; El Andaloussi S; Elie-Caille C; Erdbrugger U; Falcon-Perez JM; Fatima F; Fish JE; Flores-Bellver M; Forsonits A; Frelet-Barrand A; Fricke F; Fuhrmann G; Gabrielsson S; Gamez-Valero A; Gardiner C; Gartner K; Gaudin R; Gho YS; Giebel B; Gilbert C; Gimona M; Giusti I; Goberdhan DC; Gorgens A; Gorski SM; Greening DW; Gross JC; Gualerzi A; Gupta GN; Gustafson D; Handberg A; Haraszti RA; Harrison P; Hegyesi H; Hendrix A; Hill AF; Hochberg FH; Hoffmann KF; Holder B; Holthofer H; Hosseinkhani B; Hu G; Huang Y; Huber V; Hunt S; Ibrahim AG; Ikezu T; Inal JM; Isin M; Ivanova A; Jackson HK; Jacobsen S; Jay SM; Jayachandran M; Jenster G; Jiang L; Johnson SM; Jones JC; Jong A; Jovanovic-Talisman T; Jung S; Kalluri R; Kano SI; Kaur S; Kawamura Y; Keller ET; Khamari D; Khomyakova E; Khvorova A; Kierulf P; Kim KP; Kislinger T; Klingeborn M; Klinke DJ 2nd; Kornek M; Kosanovic MM; Kovacs AF; Kramer-Albers EM; Krasemann S; Krause M; Kurochkin IV; Kusuma GD; Kuypers S; Laitinen S; Langevin SM; Languino LR; Lannigan J; Lasser C; Laurent LC; Lavieu G; Lazaro-Ibanez E; Le Lay S; Lee MS; Lee YXF; Lemos DS; Lenassi M; Leszczynska A; Li IT; Liao K; Libregts SF; Ligeti E; Lim R; Lim SK; Line A; Linnemannstons K; Llorente A; Lombard CA; Lorenowicz MJ; Lorincz AM; Lotvall J; Lovett J; Lowry MC; Loyer X; Lu Q; Lukomska B; Lunavat TR; Maas SL; Malhi H; Marcilla A; Mariani J; Mariscal J; Martens-Uzunova ES; Martin-Jaular L; Martinez MC; Martins VR; Mathieu M; Mathivanan S; Maugeri M; McGinnis LK; McVey MJ; Meckes DG Jr.; Meehan KL; Mertens I; Minciacchi VR; Moller A; Moller Jorgensen M; Morales-Kastresana A; Morhayim J; Mullier F; Muraca M; Musante L; Mussack V; Muth DC; Myburgh KH; Najrana T; Nawaz M; Nazarenko I; Nejsum P; Neri C; Neri T; Nieuwland R; Nimrichter L; Nolan JP; Nolte-'t Hoen EN; Noren Hooten N; O'Driscoll L; O'Grady T; O'Loghlen A; Ochiya T; Olivier M; Ortiz A; Ortiz LA; Osteikoetxea X; Ostergaard O; Ostrowski M; Park J; Pegtel DM; Peinado H; Perut F; Pfaffl MW; Phinney DG; Pieters BC; Pink RC; Pisetsky DS; Pogge von Strandmann E; Polakovicova I; Poon IK; Powell BH; Prada I; Pulliam L; Quesenberry P; Radeghieri A; Raffai RL; Raimondo S; Rak J; Ramirez MI; Raposo G; Rayyan MS; Regev-Rudzki N; Ricklefs FL; Robbins PD; Roberts DD; Rodrigues SC; Rohde E; Rome S; Rouschop KM; Rughetti A; Russell AE; Saa P; Sahoo S; Salas-Huenuleo E; Sanchez C; Saugstad JA; Saul MJ; Schiffelers RM; Schneider R; Schoyen TH; Scott A; Shahaj E; Sharma S; Shatnyeva O; Shekari F; Shelke GV; Shetty AK; Shiba K; Siljander PR; Silva AM; Skowronek A; Snyder OL 2nd; Soares RP; Sodar BW; Soekmadji C; Sotillo J; Stahl PD; Stoorvogel W; Stott SL; Strasser EF; Swift S; Tahara H; Tewari M; Timms K; Tiwari S; Tixeira R; Tkach M; Toh WS; Tomasini R; Torrecilhas AC; Tosar JP; Toxavidis V; Urbanelli L; Vader P; van Balkom BW; van der Grein SG; Van Deun J; van Herwijnen MJ; Van Keuren-Jensen K; van Niel G; van Royen ME; van Wijnen AJ; Vasconcelos MH; Vechetti IJ Jr.; Veit TD; Vella LJ; Velot E; Verweij FJ; Vestad B; Vinas JL; Visnovitz T; Vukman KV; Wahlgren J; Watson DC; Wauben MH; Weaver A; Webber JP; Weber V; Wehman AM; Weiss DJ; Welsh JA; Wendt S; Wheelock AM; Wiener Z; Witte L; Wolfram J; Xagorari A; Xander P; Xu J; Yan X; Yanez-Mo M; Yin H; Yuana Y; Zappulli V; Zarubova J; Zekas V; Zhang JY; Zhao Z; Zheng L; Zheutlin AR; Zickler AM; Zimmermann P; Zivkovic AM; Zocco D; Zuba-Surma EK, J Extracell Vesicles 2018, 7 (1), 1535750. DOI 10.1080/20013078.2018.1535750. [PubMed: 30637094]

40. Norris SCP; Soto J; Kasko AM; Li S, ACS Appl Mater Interfaces 2021. DOI 10.1021/acsami.0c19627.
41. Weigelin B; Bakker G-J; Friedl P, IntraVital 2012, 1 (1), 32–43. DOI 10.4161/intv.21223. [PubMed: 29607252]
42. Paul CD; Hung WC; Wirtz D; Konstantopoulos K, Annu Rev Biomed Eng 2016, 18, 159–80. DOI 10.1146/annurev-bioeng-071114-040654. [PubMed: 27420571]
43. Hennig K; Wang I; Moreau P; Valon L; DeBeco S; Coppey M; Miroshnikova YA; Albiges-Rizo C; Favard C; Voituriez R; Balland M, Science Advances 2020, 6 (1), eaau5670. DOI 10.1126/sciadv.aau5670. [PubMed: 31921998]
44. Malet-Engra G; Yu W; Oldani A; Rey-Barroso J; Gov Nir S.; Scita G; Dupré L, Current Biology 2015, 25 (2), 242–250. DOI 10.1016/j.cub.2014.11.030. [PubMed: 25578904]
45. Palecek SP; Loftus JC; Ginsberg MH; Lauffenburger DA; Horwitz AF, Nature 1997, 385 (6616), 537–540. DOI 10.1038/385537a0. [PubMed: 9020360]

46. Cui K; Ardell CL; Podolnikova NP; Yakubenko VP, Frontiers in immunology 2018, 9, 2650–2650. DOI 10.3389/fimmu.2018.02650. [PubMed: 30524429]
47. Beaune G; Blanch-Mercader C; Douezan S; Dumond J; Gonzalez-Rodriguez D; Cuvelier D; Ondarçuhu T; Sens P; Dufour S; Murrell MP; Brochard-Wyart F, Proceedings of the National Academy of Sciences 2018, 115 (51), 12926–12931. DOI 10.1073/pnas.1811348115.
48. Zajac O; Raingeaud J; Libanje F; Lefebvre C; Sabino D; Martins I; Roy P; Benatar C; Canet-Jourdan C; Azorin P; Polrot M; Gonin P; Benbarche S; Souquere S; Pierron G; Nowak D; Bigot L; Ducreux M; Malka D; Lobry C; Scoazec J-Y; Eveno C; Pocard M; Perfettini J-L; Elias D; Dartigues P; Goéré D; Jaulin F, Nature Cell Biology 2018, 20 (3), 296–306. DOI 10.1038/s41556-017-0027-6. [PubMed: 29403038]
49. Liu Y-J; Le Berre M; Lautenschlaeger F; Maiuri P; Callan-Jones A; Heuzé M; Takaki T; Voituriez R; Piel M, Cell 2015, 160 (4), 659–672. DOI 10.1016/j.cell.2015.01.007. [PubMed: 25679760]
50. Pagès D-L; Dornier E; De Seze J; Wang L; Luan R; Cartry J; Canet-Jourdan C; Raingeaud J; Voituriez R; Coppey M; Piel M; Jaulin F, bioRxiv 2020, 2020.05.28.106203. DOI 10.1101/2020.05.28.106203.
51. Shields CW; Evans MA; Wang LL-W; Baugh N; Iyer S; Wu D; Zhao Z; Pusuluri A; Ukidve A; Pan DC; Mitragotri S, Science Advances 2020, 6 (18), eaaz6579. DOI 10.1126/sciadv.aaz6579. [PubMed: 32494680]
52. Montell DJ; Yoon WH; Starz-Gaiano M, Nature Reviews Molecular Cell Biology 2012, 13 (10), 631–645. DOI 10.1038/nrm3433. [PubMed: 23000794]
53. Cai D; Dai W; Prasad M; Luo J; Gov NS; Montell DJ, Proceedings of the National Academy of Sciences 2016, 113 (15), E2134–E2141. DOI 10.1073/pnas.1522656113.
54. Lin R-Z; Chang H-Y, Biotechnology Journal 2008, 3 (9–10), 1172–1184. DOI 10.1002/biot.200700228. [PubMed: 18566957]
55. Lee W; Kalashnikov N; Mok S; Halaoui R; Kuzmin E; Putnam AJ; Takayama S; Park M; McCaffrey L; Zhao R; Leask RL; Moraes C, Nature Communications 2019, 10 (1), 144. DOI 10.1038/s41467-018-07967-4.
56. Overholtzer M; Brugge JS, Nature Reviews Molecular Cell Biology 2008, 9 (10), 796–809. DOI 10.1038/nrm2504. [PubMed: 18784728]
57. Haeger A; Wolf K; Zegers MM; Friedl P, Trends in Cell Biology 2015, 25 (9), 556–566. DOI 10.1016/j.tcb.2015.06.003. [PubMed: 26137890]
58. Dai W; Guo X; Cao Y; Mondo JA; Campanale JP; Montell BJ; Burrous H; Streichan S; Gov N; Rappel W-J; Montell DJ, Science 2020, 370 (6519), 987–990. DOI 10.1126/science.aaz4741. [PubMed: 33214282]
59. Paul CD; Shea DJ; Mahoney MR; Chai A; Laney V; Hung W-C; Konstantopoulos K, The FASEB Journal 2016, 30 (6), 2161–2170. DOI 10.1096/fj.201500199R. [PubMed: 26902610]
60. Thompson AJ; Pillai EK; Dimov IB; Foster SK; Holt CE; Franze K, Elife 2019, 8. DOI 10.7554/eLife.39356.
61. Zanotelli MR; Rahman-Zaman A; VanderBurgh JA; Taufalele PV; Jain A; Erickson D; Bordeleau F; Reinhart-King CA, Nature Communications 2019, 10 (1), 4185. DOI 10.1038/s41467-019-12155-z.
62. Jakobsson L; Franco CA; Bentley K; Collins RT; Ponsioen B; Aspalter IM; Rosewell I; Busse M; Thurston G; Medvinsky A; Schulte-Merker S; Gerhardt H, Nature Cell Biology 2010, 12 (10), 943–953. DOI 10.1038/ncb2103. [PubMed: 20871601]
63. Amaro A; Angelini G; Mirisola V; Esposito AI; Reverberi D; Matis S; Maffei M; Giaretti W; Viale M; Gangemi R; Emionite L; Astigiano S; Cilli M; Bachmeier BE; Killian PH; Albini A; Pfeffer U, Oncotarget 2016, 7 (42), 68803–68820. DOI 10.18632/oncotarget.11931. [PubMed: 27626697]
64. Liu C; Zhang Y; Lim S; Hosaka K; Yang Y; Pavlova T; Alkasalias T; Hartman J; Jensen L; Xing X; Wang X; Lu Y; Nie G; Cao Y, Clinical Cancer Research 2017, 23 (16), 4769–4779. DOI 10.1158/1078-0432.ccr-17-0101. [PubMed: 28420724]
65. Norris SCP; Delgado SM; Kasko AM, Polymer Chemistry 2019, 10 (23), 3180–3193. DOI 10.1039/C9PY00308H.
66. Mott PH; Roland CM, Physical Review B 2009, 80 (13), 132104. DOI 10.1103/PhysRevB.80.132104.

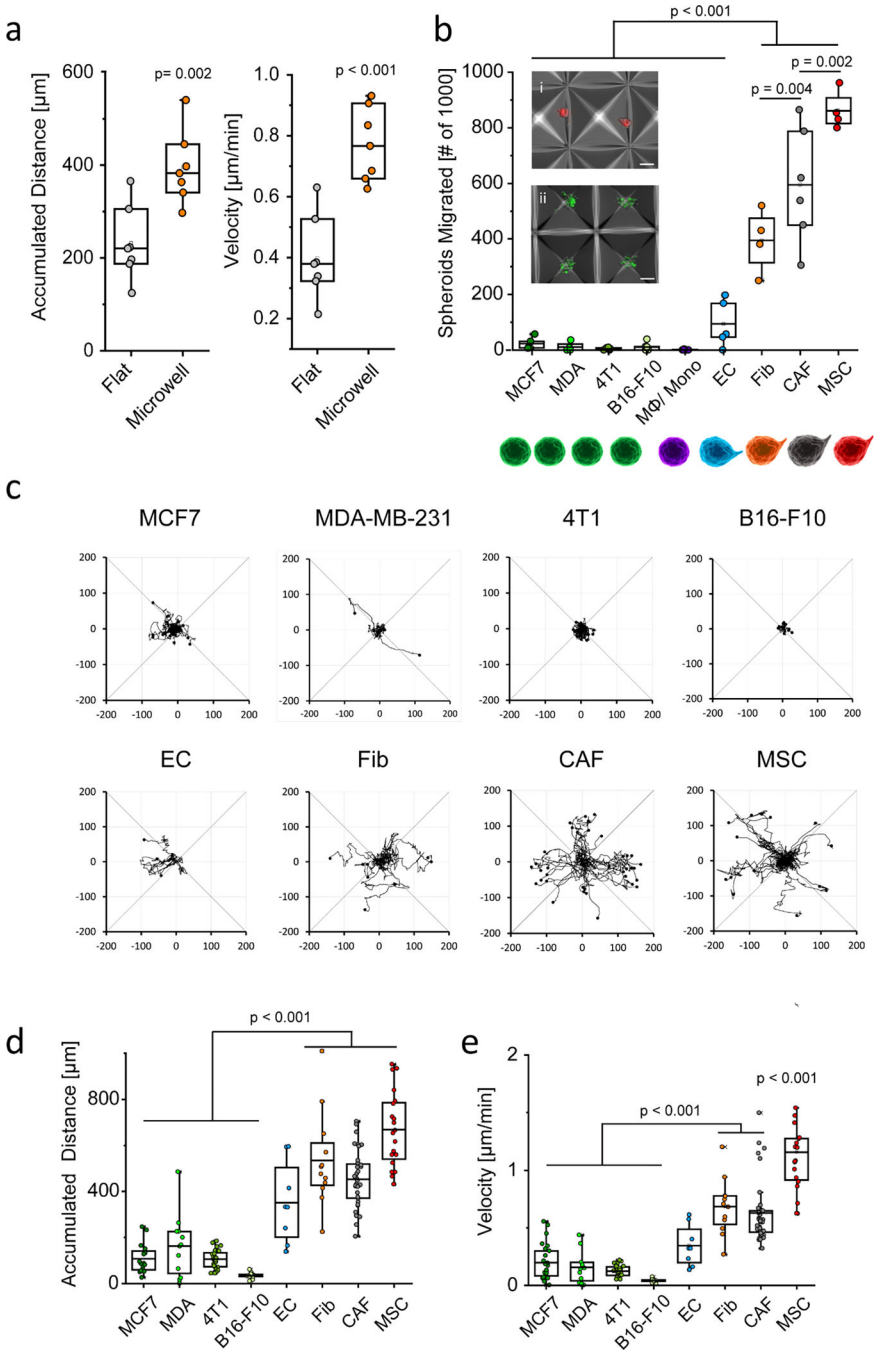

Figure 1. Differences in the migration of spheroids formed by single cell types.

(a) Accumulated distance and velocity of fibroblast spheroids migrating on flat low-adhesive surface and on microwell surface. **(b)** Number of spheroids migrated to the top of low-adhesive microwells after 24 hours for human breast cancer cell lines (MCF7 and MDA-MB-231), mouse breast cancer cell line 4T1, and melanoma cancer cell line B16-F10, monocytes or macrophages, endothelial cells (ECs), fibroblasts (Fib), CAFs and MSCs. i - MSC spheroids migrated to the top of the microwells after 24 hours; ii - cancer cell aggregated in the low-adhesive microwells after 24 hours with no displacement observed,

scale bar = 100 μm. **(c)** Migration trajectories of spheroids in the microwells evaluated from time-lapse microscopy videos, the cross represents the edges of the inverted pyramidal microwell. **(d)** Total distance migrated by the spheroids. **(e)** Comparison of speed of different spheroids formed by single cell types.

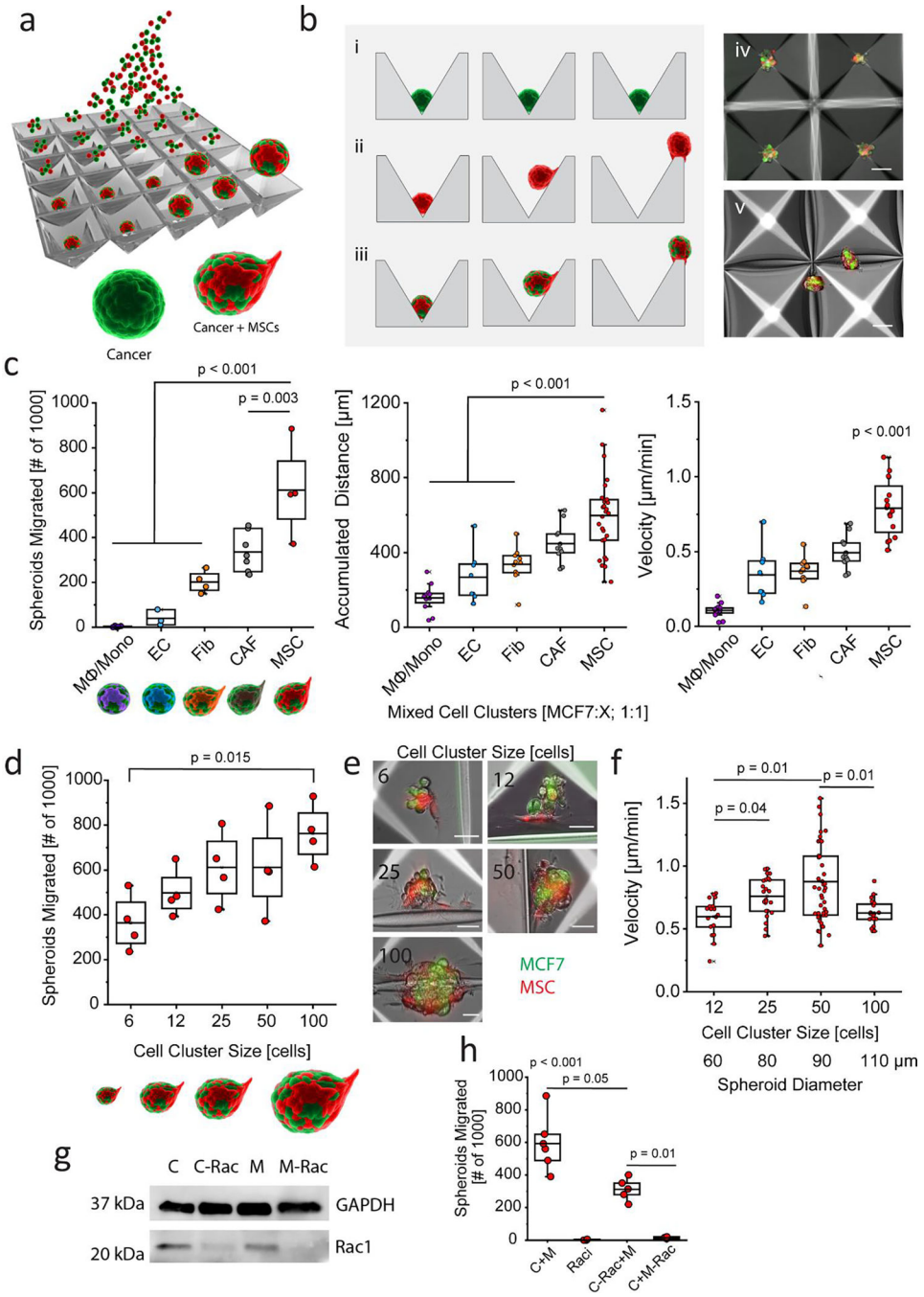

Figure 2. Differences in the migration of mixed spheroids composed of two cell types.

(a) Schematics of spheroid formation in the low-adhesive microwells. **(b)** Migratory behavior of spheroids composed of different cell types, i - non-migratory cancer cell clusters, ii - migratory MSC clusters, iii - mixed spheroids of cancer cells (green) and MSCs (red), iv - visualization of non-migratory mixed spheroids in the microwells, v – migratory cell aggregates reaching the top of the microwells in 24 hours. Scale bar = 100 µm. **(c)** Quantification of mixed spheroid migration by counting spheroid numbers that reached the top of the microwell in 24 hours. Accumulated distance and velocity of spheroids were

evaluated from time-lapse videos. Spheroids in this experiment were formed by MCF7 cancer cells and other cell type in a ratio 1:1. **(d)** The migration of different sizes of mixed cell clusters formed by MCF7 cancer cells and MSCs in the ratio 1:1 evaluated by endpoint assessment of numbers of spheroids that reached the top of the microwell in 24 hours. **(e)** Cell clusters of 6 to 100 cells formed by cancer cells (green) and MSCs (red) in a ratio 1:1, scale bar – 50 μm. **(f)** Velocity of MSC clusters of different sizes. **(g)** Quantification of migration of spheroids composed of MCF7+MSCs (C+M), spheroids of MCF7+MSCs in the presence of ROCK inhibitor (ROCKi) or Rac inhibitor (Raci), spheroids of MCF7 cancer cells with Rac1 knockdown and normal MSCs (C-Rac+M), and spheroids of normal MCF7 cancer cells. and MSCs with Rac knockdown (C+M-Rac) C: cancer cell; M: MSC. **(h)** Western blot showing a successful knockdown of Rac1 in MCF7 cancer cells (C-Rac) and MSCs (M-Rac).

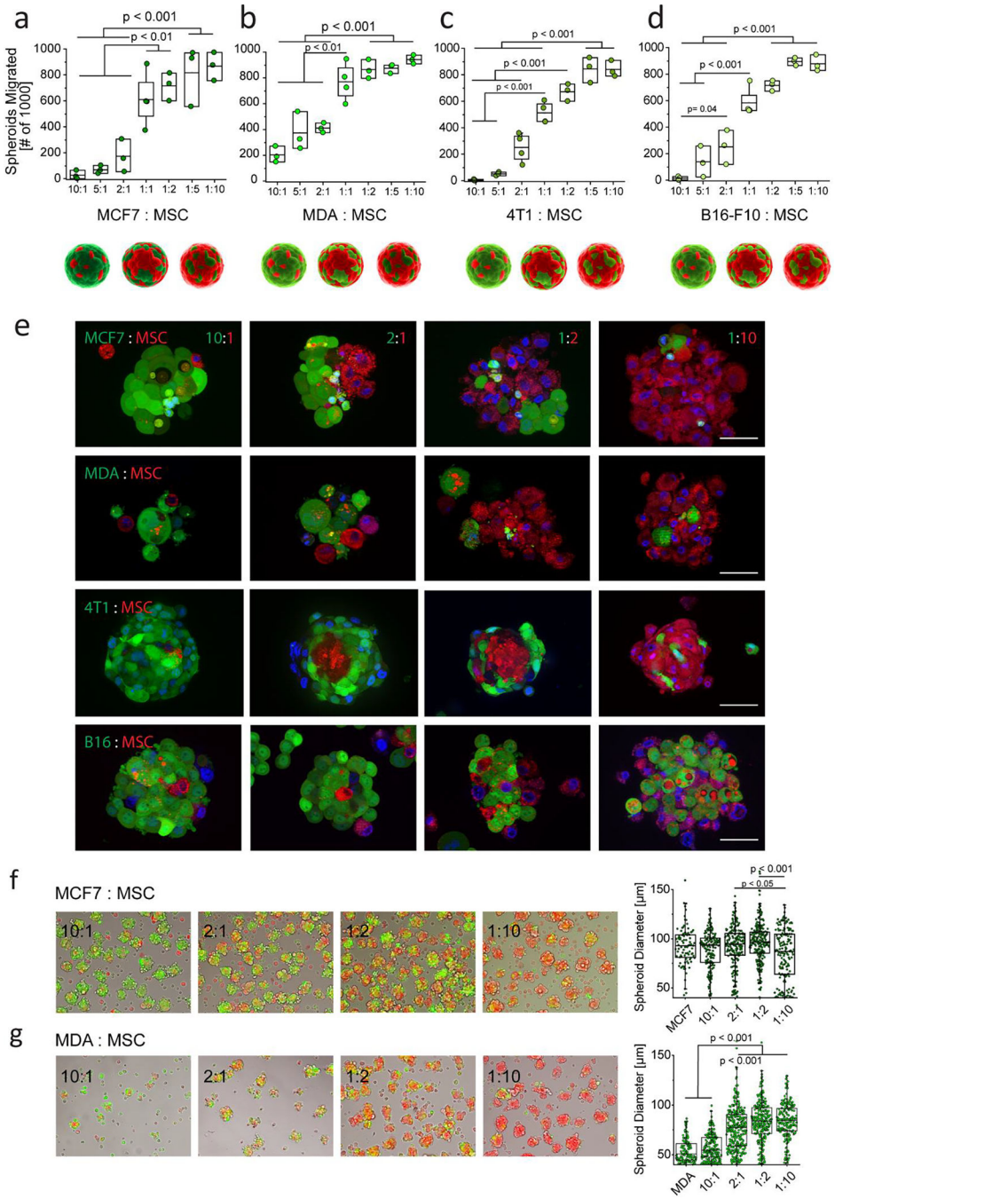

Figure 3. Variation in the cell cluster composition affected cell migration and organization.

(a) Numbers of migrating spheroids composed of different ratios of MCF7 cancer cells and MSCs after 24 hours. **(b)** Numbers of spheroids that migrated to the top of the microwell in 24 hours. Spheroids were composed of different ratios of MDA-MB-231 cancer cells and MSCs. **(c)** Numbers of migrating spheroids composed of different ratios of 4T1 cancer cells to MSCs after 24 hours. **(d)** Numbers of migrating spheroids composed of different ratios of B16-F10 cancer cells to MSCs after 24 hours. **(e)** Composition of spheroids formed by MCF7, MDA-MB-231, 4T1, and B16-F10 cancer cells (green) with MSCs (red) after 2 days

in culture. Scale bar = 50 μm. **(f)** MCF7:MSC spheroids of different ratios were harvested from the microwells after 24 hours; cancer cells -green, MSCs – red; spheroid size was not different among groups. **(g)** MDA:MSC spheroids of different ratios were harvested from the microwells after 24 hours. The samples containing more MDA than MSCs stayed as single cells or formed smaller spheroids. The ability to form spheroids increased with the number of MSCs in the cluster.

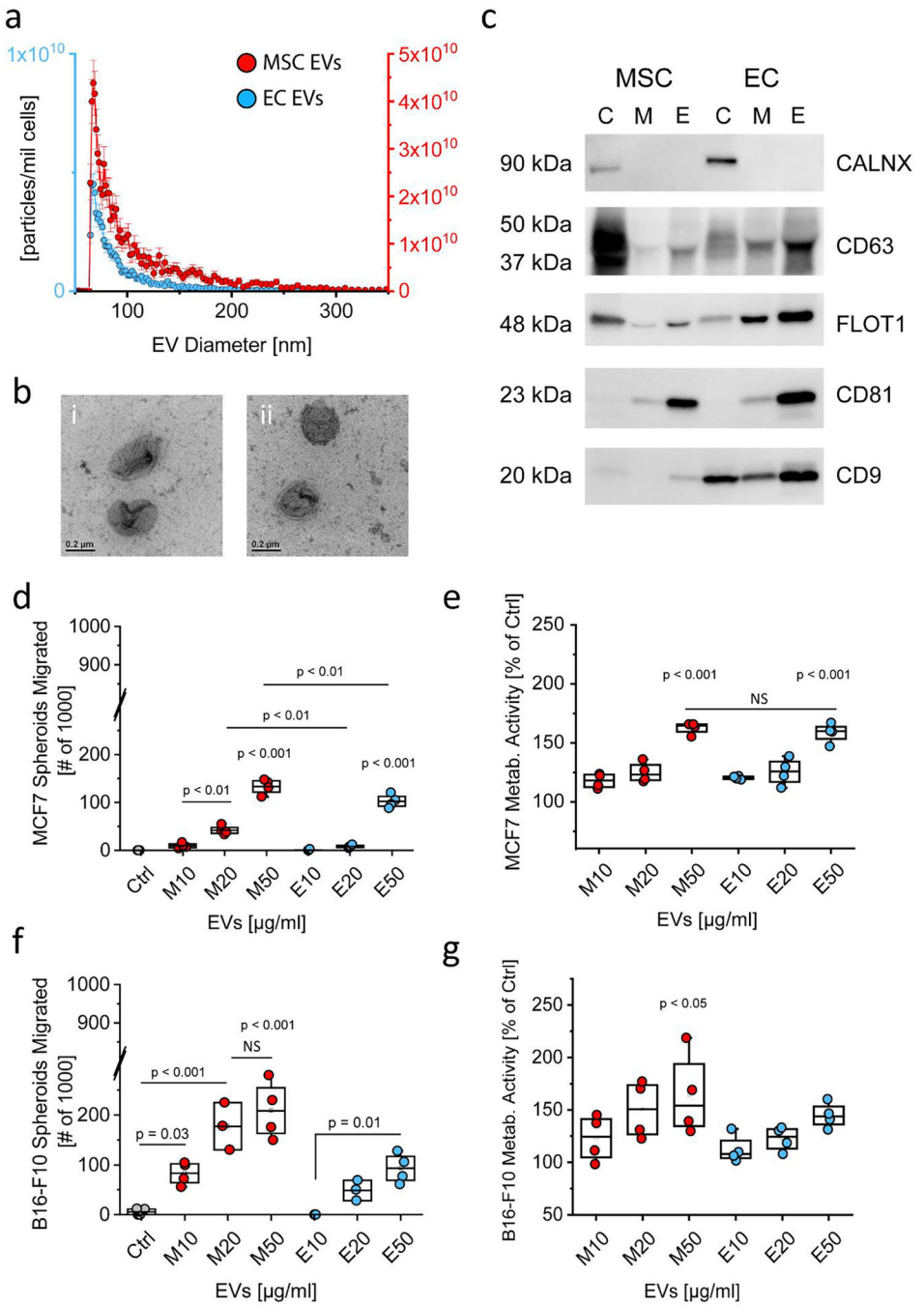

Figure 4. The effect of EVs secreted by MSCs or ECs on cancer spheroid migration and growth.

(a) EV size and concentration measured by microfluidic resistive pulse sensing. **(b)** TEM images of EVs secreted by MSCs (i) and ECs (ii). **(c)** Western blotting analysis of EVs secreted by MSCs and ECs, C – cell lysate, M – microvesicles, E – EVs. **(d)** Number of migrating MCF7 cancer spheroids after 24-hour incubation with 10, 20 or 50 µg/ml of MSC EVs (M10, M20 or M50 respectively) or EC EVs (E10, E20 or E50 respectively). Ctrl – control, medium without EVs was added. **(e)** Metabolic activity of MCF7 spheroids after 48-hour incubation with different concentrations of EVs. **(f)** Migration of B16-F10 cancer

spheroids after 24-hour incubation with 10, 20 or 50 μg/ml of MSC EVs or EC EVs. Ctrl – control, medium without EVs was added. **(g)** Metabolic activity of B16-F10 spheroids after 48-hour incubation with different concentrations of EVs.

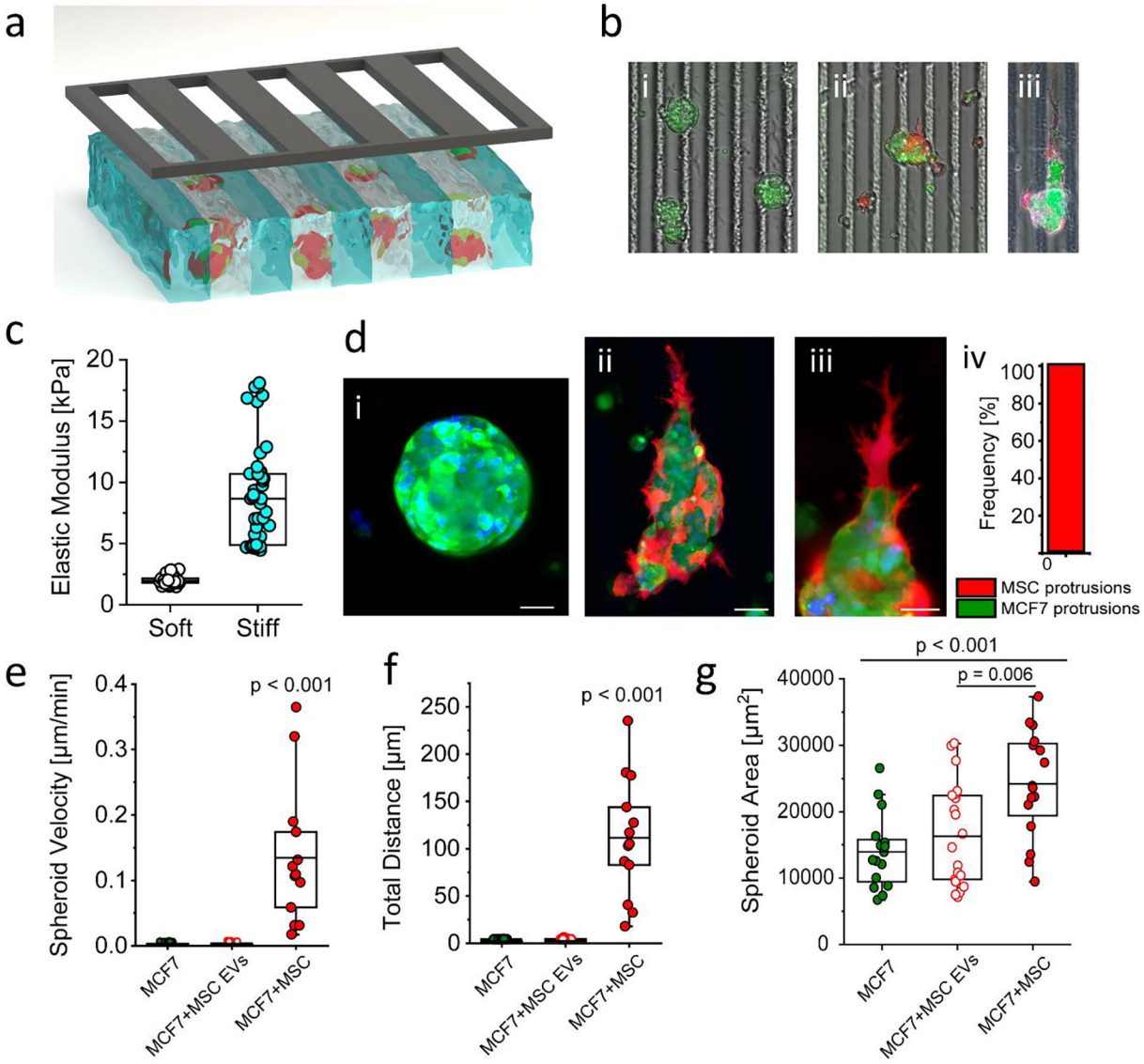

Figure 5. Cell cluster behavior in the micropatterned hydrogel with stripes of two different stiffnesses.

(a) Schematics of micropatterned GelMA hydrogel with embedded spheroids fabricated with the use of photomask that blocks UV irradiation, resulting softer stripes. **(b)** Visualization of spheroids embedded in the striped hydrogel. i – MCF7 (green) cancer spheroids after 7 days in culture, ii – MCF7 (green) +MSC (red) spheroid after 2 days, and iii - MCF7+MSC spheroid after 7 days in culture, with MSCs acting like tip cells guiding the migration. **(c)** Elastic modulus of stripes of different stiffnesses measured by AFM. **(d)** Confocal images of spheroids after 7 days in culture. i – MCF7 (green) spheroid, ii – MCF7 (green) +MSC (red) spheroid, scale bar – 50 µm, iii – detail of MSC tip cell in MCF7+MSC spheroid, scale bar – 25 µm. iv – Quantification shows frequency of MSC vs. MCF7 protrusions per mixed spheroid. In all cases (100%, 20/20 MCF7+MSC spheroids), MSC were the only cells extending protrusions. **(e)** Spheroid velocity in micropatterned hydrogel **(f)** Distance migrated by spheroids in 24 hours. **(g)** Spheroid area after 7 days in culture.

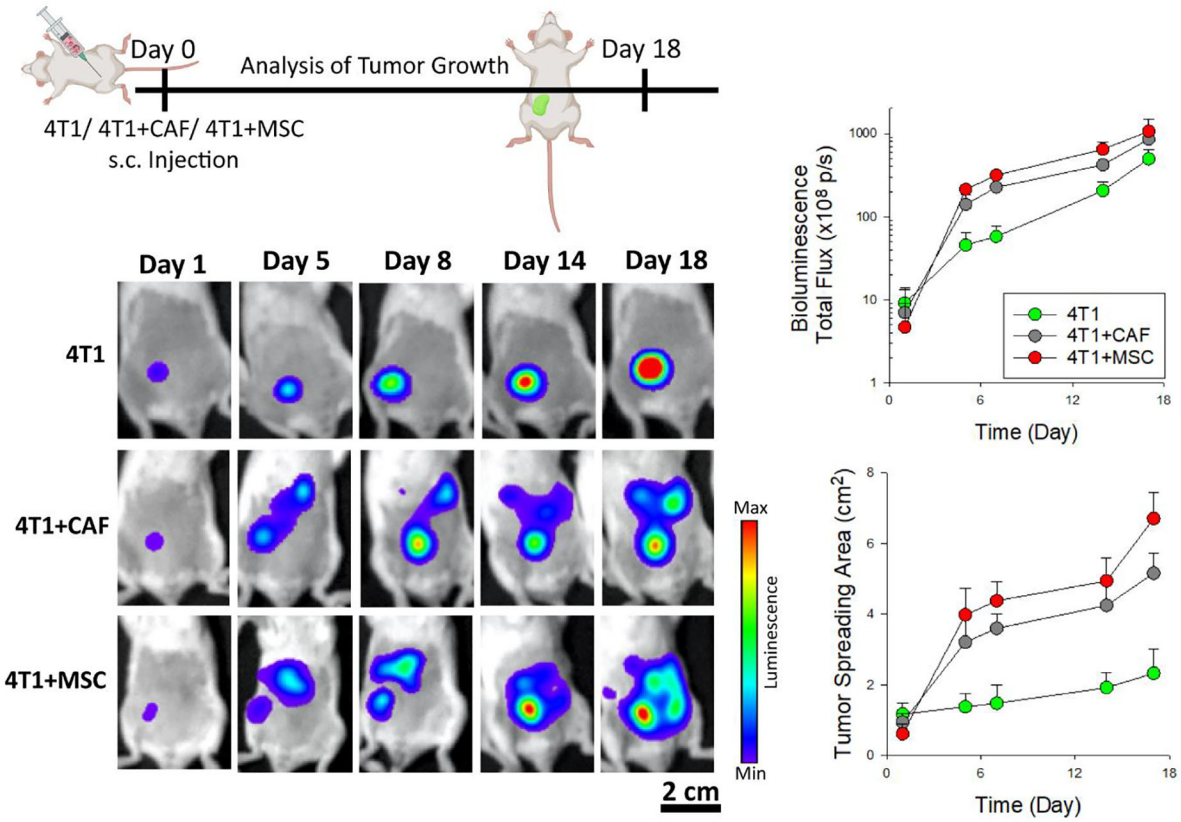

Figure 6. Evaluation of cancer cell growth and spreading in mouse breast cancer model.

Evaluation of cancer cell growth and spreading in mouse breast cancer model. Spheroids of luciferase-expressing 4T1 breast cancer cells with or without MSCs or CAFs were injected subcutaneously into balb/c wild-type mice, and the tumor growth was monitored by measuring and quantifying the in vivo bioluminescence signal with the IVIS imaging system. Sequential bioluminescence imaging was used to quantify the growth and spreading of tumor over time.